

# Quantifying the Preferential Direction of the Model Gradient in Adversarial Training With Projected Gradient Descent

Ricardo Bigolin Lanfredi<sup>1</sup> Joyce D. Schroeder<sup>2</sup> Tolga Tasdizen<sup>1</sup>

## Abstract

Adversarial training, especially projected gradient descent (PGD), has been a successful approach for improving robustness against adversarial attacks. After adversarial training, gradients of models with respect to their inputs have a preferential direction. However, the direction of alignment is not mathematically well established, making it difficult to evaluate quantitatively. We propose a novel definition of this direction as the direction of the vector pointing toward the closest point of the support of the closest inaccurate class in decision space. To evaluate the alignment with this direction after adversarial training, we apply a metric that uses generative adversarial networks to produce the smallest residual needed to change the class present in the image. We show that PGD-trained models have a higher alignment than the baseline according to our definition, that our metric presents higher alignment values than a competing metric formulation, and that enforcing this alignment increases the robustness of models.

## 1. Introduction

Deep learning models have been shown to suffer from a lack of robustness against directed attacks that produce only small perturbations to the original input (Goodfellow et al., 2015). Several attacks of varying strengths have been proposed (Xu et al., 2020). To solve the lack of robustness, researchers have proposed several methods for defending against such attacks (Xu et al., 2020). These defenses include, for instance, training using adversarial examples as samples (Goodfellow et al., 2015; Madry et al., 2018; Zhang et al., 2019), preprocessing input data (Guo et al., 2018; Samangouei et al., 2018; Nandy et al., 2020), regularizing gradients (Lyu et al., 2015; Hein & Andriushchenko, 2017; Ross & Doshi-Velez, 2018; Jakubovitz & Giryes,

2018; Finlay & Oberman, 2021), and detecting adversarial attacks (Carlini & Wagner, 2017b). One of the most successful defenses in terms of resisting new attacks (Carlini et al., 2017; Athalye et al., 2018) is projected gradient descent (PGD) training (Madry et al., 2018).

PGD has been shown to change the gradient of the loss function of a trained model with respect to inputs  $x$  (Tsipras et al., 2019). Other robust training techniques also induce similar changes, modifying the gradient of the logits of the output class (Etmann et al., 2019; Kaur et al., 2019). We focus our studies on PGD due to its success and widespread use (Carlini et al., 2017; Madry et al., 2018; Athalye et al., 2018), but our theoretical analysis is generic for any robust model. Only a few quantitative studies have related gradient direction to robustness. We propose a novel definition for this direction in classification problems. We formulate a gradient alignment metric  $\alpha_{\Delta x}$  for a given sample  $x$  as the expected cosine similarity between  $\nabla \ell(x)$  and  $\Delta x$ . We define  $\nabla \ell(x)$  as the gradient with respect to input  $x$  of the function  $\ell(x)$ , related to the logits of a model and defined later in the paper, and  $\Delta x$  as the vector pointing from  $x$  to its closest neighbor  $x'$  in the support of class  $\tilde{c}(x)$ . The class  $\tilde{c}(x)$  is the closest to  $x$  in decision space that is not its ground truth class.

We start by analyzing the robustness of models in a toy dataset where the data for each class lies in one of two concentric spheres, inspired by the work of Gilmer et al. (2018). The dataset was used by Gilmer et al. (2018) to demonstrate that non-zero generalization error can be the only cause of adversarial examples. Nonetheless, we use the dataset to prove a proportional relation between robustness and the proposed alignment metric. The theorems used for this proof are generic for multiclass classification problems, assuming local linearity and specific characteristics of the data distribution. Since  $x'$  is not straightforward to calculate for complex datasets, we also propose two methods to calculate an approximation  $\hat{x}'$  by applying generative adversarial training (Goodfellow et al., 2014). We proceed to evaluate if the metric provides information for more complex datasets. Our results show that even though the most robust model did not always match the model with closer alignment, compared to a baseline, robust models trained with PGD have

<sup>1</sup>Scientific Computing and Imaging Institute, University of Utah, Salt Lake City, USA <sup>2</sup>Department of Radiology and Imaging Sciences, University of Utah, Salt Lake City, USA. Correspondence to: Ricardo Bigolin Lanfredi <ricbl@sci.utah.edu>.

a larger average  $\alpha_{\Delta x}$ , and models trained using  $\alpha_{\Delta x}$  for enforcing a penalty on its gradient have higher robustness. Furthermore, the proposed metric show a closer alignment for robust models than an existing alignment metric proposed by Etmann et al. (2019).

### 1.1. Related work

Etmann et al. (2019) mathematically defined the alignment of gradients after robust training as the alignment between the input image  $x$  and the gradient of the logits of the output class  $m(x)$  with respect to  $x$ ,  $\nabla \text{logit}(x)_{m(x)}$ . Robustness is shown to be bounded by the sum of the given metric with other terms related to gradients and internal bias weights. However, the theoretical approach for the bias terms in the linear approximation of a model leads to a relatively loose bound in the relationship between robustness and alignment. We compare the metric proposed by Etmann et al. (2019) against our metric and demonstrate that ours presents a closer alignment in practice. In analyses of Ilyas et al. (2019) and Tanay & Griffin (2016), the gradient of robust models is shown to be better aligned with the vector connecting the centroid of two classes than the gradients of non-robust models. However, this finding is restricted to binary linear models. The complex boundaries of piecewise linear deep learning models are unlikely to benefit from pointing in a single direction over the entire support of classes in high-dimensional datasets. Using local information of projection to the support of the opposite class, as we propose, is required to get flexible directions for each locally linear region of the model.

To study the gradients' alignment, we introduce a metric and propose to evaluate its correlation with robustness. Other metrics with similar motivations have been studied. The local linearity measure (LLM) (Qin et al., 2019), for which a low value represents high local linearity of models around data points, is inversely correlated with the number of iterations in PGD. The metric was not evaluated directly against robustness, despite its potential. The CLEVER metric (Weng et al., 2018) uses an estimated extreme value for the Lipschitz constant of the model to calculate a lower bound for robustness without having to perform evaluation attacks. This metric complements ours because it evaluates gradient magnitude instead of gradient direction.

We propose a penalty on the direction of  $\nabla_{\ell(x)}$ . This proposal adds to the literature of gradient penalties for robustness. Regularizing the gradient of a model with respect to its inputs has repeatedly been shown to increase its robustness (Lyu et al., 2015; Ross & Doshi-Velez, 2018; Hein & Andriushchenko, 2017; Jakubovitz & Giryas, 2018; Finlay & Oberman, 2021). However, this penalty does not penalize the direction of the gradient. The local linearity regularizer (LLR) (Qin et al., 2019) was proposed and com-

bined with PGD to allow faster training. Given that  $\mathcal{L}(x)$  is the cross-entropy loss function, this penalty is equivalent to enforcing the  $\nabla_{\mathcal{L}(x)}$  vector to be constant around data samples. However, the penalty enforces no direction. A penalty for aligning  $\nabla \text{logit}(x)_{m(x)}$  with  $x$  was proposed by Etmann et al. (2019), only as a future work. An analogous penalty was proposed by Chan et al. (2020b). The alignment proposed by Noack et al. (2021) enforces the proximity between a saliency map of the non-robust model generated through SmoothGrad (Smilkov et al., 2017), a visual attribution technique, and  $\nabla \text{logit}(x)_y$ , where  $y$  is the ground truth class for  $x$ . No theoretical justification for the choice of direction generated through such a technique was given.

Other works study the relationship between a model's gradient and its robustness without directly studying the direction to which the gradient aligns. The method proposed by Chan et al. (2020a) transfers robustness from one model trained with PGD to other models by enforcing similar  $\nabla_{\mathcal{L}(x)}$ . Boopathy et al. (2020) show that using their method to train models to have robust interpretation saliency maps indirectly leads to robust classification decisions. Helland & VanHoudnos (2020) qualitatively indicates that the gradient changes when performing robust training are a consequence of smoothness regularization over a model's decision functions in conjunction with the decision boundary orientation caused by conventional classification losses.

## 2. Approach

### 2.1. Motivation and formulation of alignment metric

The robustness of a decision model  $m$  at a specific point  $x$  can be defined as the signed distance of  $x$  to the closest point where it is associated with a different model output. Formally, we define

$$\rho(x) = \begin{cases} \inf\{\|\delta\|_p : m(x + \delta) \neq y\}, & \text{if } m(x) = y \\ -\inf\{\|\delta\|_p : m(x + \delta) = y\}, & \text{if } m(x) \neq y \end{cases} \quad (1)$$

where  $\rho(x)$  is the robustness of  $m$  against adversarial attacks at point  $x$ , and  $y$  is the ground truth class associated with  $x$ . We set a negative distance for misclassified examples to penalize errors and prevent models with a trivial decision boundary, i.e., one that always assigns the same class, to have infinite expected robustness. For this analysis, we will use the  $L^2$  norm, i.e.,  $p = 2$ .

We analyze the *Spheres* dataset proposed by Gilmer et al. (2018) to hypothesize about a specific aspect of robustness: the association between the robustness of a decision model and the direction of the gradient of its logits with respect to its inputs. We use this dataset because its simplicity allows for a more accessible analysis, while Deep ReLU

networks can still fail in modeling it robustly (Gilmer et al., 2018). The *Spheres* dataset is composed of two classes with support on the surface of two hyperspheres, of radius 1.0 (class -1) and 1.3 (class 1), in a 500-dimensional space. The prior probability for each class is 0.5, and the distribution of samples is uniform on each hypersphere surface. We use the term support of a class  $c$  as defined by  $\text{supp}_c = \{x \in X \mid P(x|y = c) > 0\}$ , where  $X$  is the domain of inputs.

For this dataset, the optimally robust model  $m_p$  has its decision rule defined by

$$c = \begin{cases} 1, & \text{if } \|x\|_2 > t \\ -1, & \text{if } \|x\|_2 < t \end{cases}, t = 1.15. \quad (2)$$

This model has a margin of 0.15 between the decision boundary and any data point. Note that the expected robustness  $\mathbb{E}_{x \sim X}[\rho(x)]$  is the same for all values of  $t$ , and the decision to choose  $t = 1.15$  is based on classification margins. A differentiable decision model can be obtained by defining  $\text{logit}(x)_1 = \|x\|_2 - 1.15$  and  $\text{logit}(x)_{-1} = -\|x\|_2 + 1.15$ , where  $\text{logit}(x)_c$  is the logit of a model for class  $c$  and input  $x$ . If we define a loss for the model as  $-y \times \text{logit}(x)_1 + y \times \text{logit}(x)_{-1}$ , this model has radial gradients with respect to the input. The gradients of the defined loss point toward the origin for class 1 and away from the origin for class -1. We note that the optimally robust model has gradients that point from the support of one class to the closest point  $x'$  of the support of the other class. We denote the vector connecting  $x$  to  $x'$  as  $\Delta x$ . We will proceed to theoretically justify the importance of  $\Delta x$ .

**Lemma 1.** Let  $R(x) := \sup\{r \in \mathbb{R} : \forall v \in \mathbb{R}^n \text{ s.t. } \|x - v\|_2 < r, \exists W \in \mathbb{R}^{n \times C}, \exists b \in \mathbb{R}^C \text{ s.t. } \text{logit}(v) = W^T v + b\}$ , where  $\text{logit}(v) \in \mathbb{R}^C$  is a vector representing all logits of a decision model  $m$  for input  $v$ , and  $x \in \mathbb{R}^n$ . In other words,  $R(x)$  is the radius of the largest hypersphere around  $x$  where a decision model  $m$  can be defined by a specific linear decision function. Assuming that  $R(x) \geq |\rho(x)|$  for  $m$ , then the logits of  $m$  can be modeled as a linear function, i.e.,  $\text{logit}(x) = W^T v + b$ , for robustness assessment, resulting in a robustness magnitude at  $x$  given by

$$|\rho(x)| = \min_c |\rho(x)_c| = |\rho(x)_{\tilde{c}(x)}|, \quad (3)$$

where

$$|\rho(x)_c| = \left| \frac{\text{logit}(x)_y - \text{logit}(x)_c}{\|W_{:,y} - W_{:,c(x)}\|_2} \right|, \quad (4)$$

$$\begin{aligned} \tilde{c}(x) &:= \operatorname{argmin}_{c \neq y} \{\inf\{\|v\|_2 : m(x+v) = c\}\} = \\ &= \operatorname{argmin}_{c \neq y} |\rho(x)_c| = \operatorname{argmin}_{c \neq y} \left| \frac{\text{logit}(x)_y - \text{logit}(x)_c}{\|W_{:,y} - W_{:,c(x)}\|_2} \right|, \end{aligned} \quad (5)$$

and  $W_{:,j}$  is the  $j^{\text{th}}$  column of the  $W$  matrix.

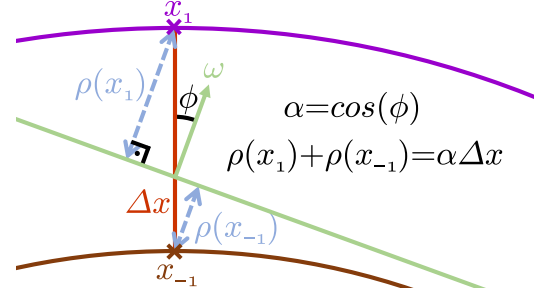


Figure 1. Illustration of the result from Theorem 1 for the *Spheres* dataset. The green straight line represents the decision boundary of an arbitrary classifier, and the purple top and brown bottom arcs represent a section of the support of classes 1 and -1, respectively. The cosine of the angle between the normal of the decision boundary ( $\omega$ ) and the vector connecting both input samples ( $\Delta x$ ) is proportional to the sum of robustnesses of both input samples.

Lemma 1 follows from Lemma 1 proposed and proved by Etmann et al. (2019). They also empirically showed that, despite  $R(x) \geq |\rho(x)|$  not holding, the linearization is a good approximation. We will refer to models satisfying the assumption in Lemma 1 as being locally linear around  $x$ .

**Theorem 1.** Let  $\text{sim}(u, v)$  be the alignment between vectors  $u$  and  $v$ , defined by their cosine similarity  $\text{sim}(u, v) = \frac{\langle u, v \rangle}{\|u\|_2 \|v\|_2}$ , let  $m$  be a classification model and let  $c^*(x) := \operatorname{argmin}_{c \neq m(x)} \{\inf\{\|v\|_2 : m(x+v) = c\}\}$ . For a pair of input examples  $x_i$  and  $x_j$ , of different classes  $i$  and  $j$ , respectively, around which  $m$  is locally linear and for which<sup>1</sup>  $\{c^*(x_i), m(x_i)\} = \{i, j\}$  and  $\{c^*(x_j), m(x_j)\} = \{i, j\}$ , the combined robustness  $\rho(x_i) + \rho(x_j)$  of  $m$  is directly proportional to  $\alpha$  according to  $\rho(x_i) + \rho(x_j) = \|x_j - x_i\|_2 \times \alpha$ , where  $\alpha = \text{sim}(x_j - x_i, \nabla \text{logit}(x_i)_j - \nabla \text{logit}(x_i)_i) = \text{sim}(x_i - x_j, \nabla \text{logit}(x_j)_i - \nabla \text{logit}(x_j)_j)$ .

Theorem 1 establishes that, given assumptions of local linearity and symmetry of closest decision boundaries, the sum of the robustness of two inputs, for which either the model's output or the closest class is the ground truth for that example, is proportional to the alignment between model gradient and a vector connecting both inputs. The proof for Theorem 1 is in Section A.2 in the Supplementary Material. An illustration of the theorem claim for the *Spheres* dataset is given in Figure 1. For use of Theorem 1 in Theorem 2, we define

$$\ell(x) := \text{logit}(x)_{\tilde{c}(x)} - \text{logit}(x)_y, \quad (6)$$

leading to  $\alpha = \text{sim}(x_{\tilde{c}(x)} - x_y, \nabla \ell(x))$ . We proceed to formulate a global metric to measure the robustness of a given model, defining it as the expected sample robustness with respect to the data distribution.

<sup>1</sup>The notation of these two equations uses sets, where  $\{a, b\} = \{i, j\}$  means that either  $a = i$  and  $b = j$ , or  $a = j$  and  $b = i$ .

**Theorem 2.** Assuming that, for a multi-class dataset of classes  $C$ ,

1. it is possible to define  $K$  mutually exclusive sets  $\mathcal{S}_k$ , each containing regions of the supports of two classes  $i_k$  and  $j_k$ , where  $\bigcup_{c \in C} \text{supp}_c = \bigcup_{k=1}^K \mathcal{S}_k$ , i.e., they cover the whole space of the support of classes;
2. for each  $\mathcal{S}_k$ , it is possible to define a bijection between the respective regions of support of classes  $i_k$  and  $j_k$  such that, given all bijection pairs  $(x_{i_k}, x_{j_k})$ ,  $x_{i_k} \in \text{supp}_{i_k}$  and  $x_{j_k} \in \text{supp}_{j_k}$ ,
  - (a)  $P(x_{i_k}) = P(x_{j_k})$ ,
  - (b) a decision model  $m$  is locally linear around  $x_{i_k}$  and  $x_{j_k}$ ;
  - (c)  $\{c^*(x_{i_k}), m(x_{i_k})\} = \{i_k, j_k\}$  and  $\{c^*(x_{j_k}), m(x_{j_k})\} = \{i_k, j_k\}$ ;

then the expected robustness of  $m$ ,  $\rho_m$ , is related to the expected alignment  $\bar{\alpha}$  between  $\nabla_{\ell(x)}$  and  $\Delta x$  of pairs  $(x_{i_k}, x_{j_k})$  over all  $\mathcal{S}_k$ , according to

$$\rho_m \geq \frac{\inf(\mathcal{D}) \times \bar{\alpha}}{2} \quad \text{and} \quad \bar{\alpha} \geq \frac{2 \times \rho_m}{\sup(\mathcal{D})}, \quad (7)$$

where  $\mathcal{D}$  is the set of distances  $\|x_{i_k} - x_{j_k}\|_2$  over all pairs  $(x_{i_k}, x_{j_k})$  over all  $\mathcal{S}_k$ .

Theorem 2 sets bounds for the relationship between the expected robustness of a model and the average alignment between the model’s gradient and vectors connecting inputs of two adjacent classes. The proof for Theorem 2 is given in Section A.2 in the Supplementary Material. The local linearity assumption of Theorem 2 is likely to hold only if the bijection can be established between the closest points of the supports of adjacent classes. Therefore, we define a metric using the concept of vector pointing to the closest point of the support of  $\tilde{c}(x)$ . This metric is given by

$$\begin{aligned} \bar{\alpha}_{\Delta x} &= \int P(x) \frac{\langle \Delta x, \nabla_{\ell(x)} \rangle}{\|\Delta x\|_2 \|\nabla_{\ell(x)}\|_2} dx, \\ \Delta x &= \underset{r}{\operatorname{arginf}} \{ \|r\|_2 : x + r \in \text{supp}_j, x \in \text{supp}_y, j \neq y \}. \end{aligned} \quad (8)$$

In practice,  $\tilde{c}(x)$  can be calculated using the linear approximation given in (5), and we propose methods for calculating  $\Delta x$  in Section 2.3. Given that assumptions from Theorem 2 are satisfied for pairs of closest points,  $\bar{\alpha}_{\Delta x}$  as defined (8) will be equal to  $\bar{\alpha}$  in (7). For the *Spheres* dataset, it is possible to establish a bijection as required by Theorem 2 using points of opposite classes along the same radial direction. Since the prior probability of both classes is balanced, and the probability distribution in both

supports is uniform,  $P(x_0) = P(x_1)$  holds for any pair of points. The assumption  $\{c^*(x_i), m(x_i)\} = \{i, j\}$  and  $\{c^*(x_j), m(x_j)\} = \{i, j\}$ ,  $i \neq j$ , always holds for binary datasets. Thus, except for a possible violation of the local linearity assumption, Theorem 2 holds for the *Spheres* dataset. Additionally, the distance between closest points is constant, so both bounds can be combined into an equality  $\rho_m = \|\Delta x\|_2 \times \bar{\alpha}_{\Delta x} / 2$ . According to Theorem 2, the optimally robust model has  $\rho_m = (0.3 \times 1) / 2 = 0.15$ , which is the expected value. However, the assumptions needed for applying Theorem 2 are unlikely to hold exactly for more complex datasets. We perform empirical analysis to evaluate the alignments of such datasets in Section 3.3. Section 3.4 provides an additional qualitative survey of the approximation defined in Lemma 1 for the models tested in Section 3.3.

## 2.2. Gradient penalty

We propose that steering  $\nabla_{\ell(x)}$  by adding a penalty  $L_\alpha$  to a supervised classification loss will increase the robustness of a model. This penalty is given by

$$L_\alpha := -\lambda_\alpha \bar{\alpha}_{\Delta x}, L = L_\alpha + \mathcal{L} \quad (9)$$

where  $\lambda_\alpha$  is a hyperparameter,  $L$  is the total loss to be optimized and  $\mathcal{L}$  is the cross-entropy loss function. This penalty is not meant to replace other robust training methods, but to show that increasing alignment increases robustness.

## 2.3. Estimating $\Delta x$

For almost all real-world datasets,  $\Delta x$  is not trivial to find. To generate it, we use generative adversarial training (Goodfellow et al., 2014) to characterize the support of classes.

### 2.3.1. DIRECT GENERATION OF $\widehat{\Delta x}$

We train a generator  $G$  to directly produce the residuals needed to convert from one class to another. The formulation draws from the VR-GAN method (Lanfredi et al., 2019), modified to work with classification tasks instead of regression tasks. For practical reasons, we use this formulation only on binary datasets. Figure 2 shows the overall formulation for training. Residuals  $\widehat{\Delta x}$  are produced according to

$$\widehat{\Delta x} = G(x, \neg y), \hat{x}' = x + \widehat{\Delta x}. \quad (10)$$

We set up an adversarial loss given by

$$\begin{aligned} L_{Dx} &= \mathbb{E} [\mathcal{L}(D(x), y)], L_{D\hat{x}'} = \mathbb{E} [\mathcal{L}(D(\hat{x}'), y)], \\ L_G &= \mathbb{E} [\mathcal{L}(D(\hat{x}'), \neg y)], \end{aligned} \quad (11)$$

where  $\mathcal{L}$  is binary cross-entropy,  $L_{Dx}$  and  $L_{D\hat{x}'}$  are losses for which a discriminator  $D$  is optimized, while  $L_G$  optimizes a generator  $G$ .  $G$  is trained to fool  $D$  ( $L_G$ ), whereas



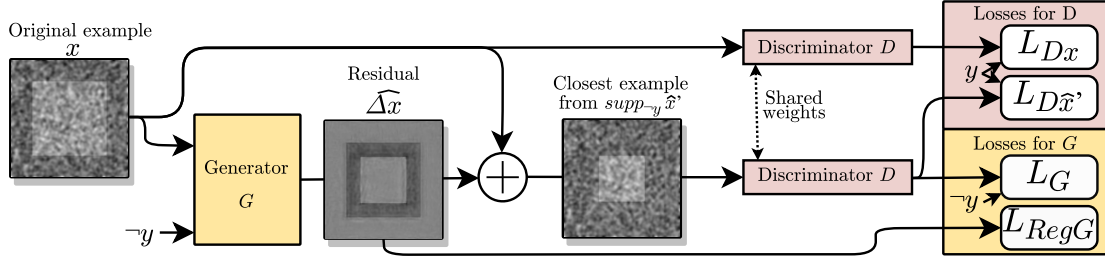


Figure 2. Training diagram for directly generating residual approximations  $\hat{\Delta}x$ . The terms  $L_{Dx_0}$ ,  $L_{D\hat{x}_0}$ , and  $L_G$  are classification losses, and  $L_{RegG}$  penalizes the length of  $\hat{\Delta}x$ .

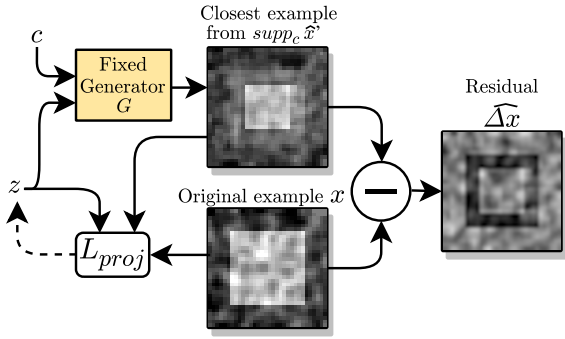


Figure 3. Diagram for indirectly generating  $\hat{\Delta}x$ . The dashed line depicts the feedback from loss  $L_{proj}$  to iteratively update  $z$ .

$D$  is trained not to be fooled ( $L_{D\hat{x}'}$ ). This adversarial setup, combined with a traditional supervised loss ( $L_{Dx}$ ), should make  $D$  accept only  $\hat{x}'$  that are in  $supp_y$ . The loss  $L_{D\hat{x}'}$  should have a smaller weight than  $L_{Dx}$  so that, if  $G$  is generating perfect modifications,  $D$  can still learn  $supp_y$ . Finally, we define the term

$$L_{RegG} = \frac{\|\hat{\Delta}x\|_2}{\sqrt{n}}, \quad (12)$$

where  $n$  is the dimensionality of  $x$ . This penalty is used to enforce that  $\hat{x}'$  is the closest point in the learned support of classes. The final optimization is given by

$$\begin{aligned} G^* &= \operatorname{argmin}_G (\lambda_G L_G + \lambda_{RegG} L_{RegG}), \\ D^* &= \operatorname{argmin}_D (\lambda_{Dx} L_{Dx} + \lambda_{D\hat{x}'} L_{D\hat{x}'}), \end{aligned} \quad (13)$$

where  $\lambda_G$ ,  $\lambda_{RegG}$ ,  $\lambda_{Dx}$ ,  $\lambda_{D\hat{x}'}$  are hyperparameters.

### 2.3.2. INDIRECT GENERATION OF $\hat{\Delta}x$

We propose an indirect method for estimating  $\Delta x$  as a strategy to scale it to multiclass datasets. This method can be easily adapted to new datasets since it uses, with no

modifications, any available established conditional GAN (cGAN) (Mirza & Osindero, 2014) for the datasets of interest. We select a cGAN proposed by Kavalerov et al. (2020), that offers competitive results for the CIFAR-10 dataset (Krizhevsky, 2009). After training a conditional generator  $G$ , we follow a similar algorithm for projection to the generative adversarial network (GAN) manifold as in the Defense-GAN method (Samangouei et al., 2018), pre-calculating the projection of all images in a dataset to all possible destination classes. In other words, we iteratively find, for each image  $x$ , the optimal latent space vector

$$z_c^* = \operatorname{argmin}_z L_{proj}(x, z, c), \quad (14)$$

where  $c$  is one of the classes of the dataset, and  $L_{proj}$  is a loss that measures both the distance between input image  $x$  and  $G(z, c)$ , and the likelihood of  $z$ , given by

$$L_{proj}(x, z, c) = \frac{\|x - G(z, c)\|_2^2}{n} + \lambda_{Regz} \frac{\|z\|_2^2}{n}. \quad (15)$$

The result of the projection,  $G(z_c^*, c)$ , is an estimation of  $x'$  for class  $c$ . We can then indirectly calculate

$$\hat{\Delta}x = G(z_c^*, \tilde{c}(x)) - x. \quad (16)$$

We use a penalty on the norm of  $z$  because a Gaussian prior was used when randomly sampling  $z$  during training for the chosen cGAN (Kavalerov et al., 2020). A representation of the algorithm can be found in Figure 3. More details of the optimization process can be found in Section A.3 in the Supplementary Material.

### 2.4. Adversarial defense and attack

Adversarial training with PGD (Madry et al., 2018) aims to find a robust parameterized classifier  $m$  by optimizing

$$\min_m \max_{\delta} \mathcal{L}(m(x + \delta), y), \|\delta\|_p < \epsilon, \quad (17)$$

where  $\delta$  is a residual with a limited norm,  $\mathcal{L}$  is a classification loss function,  $x$  is an input example,  $y$  its associated

ground truth and commonly  $p = \infty$ . The inner maximization is performed using iterative gradient ascent with  $k$  steps of size  $\eta$ . Data projections are performed after each step to satisfy norm limits and data intensity ranges. The method can also be used as a strong adversarial attack.

### 3. Experiments

We empirically analyzed<sup>2</sup> if improving the robustness of a model using PGD training increased its alignment  $\overline{\alpha_{\Delta x}}$ , and if increasing  $\overline{\alpha_{\Delta x}}$  by using the alignment penalty  $L_\alpha$  improved robustness. We compared both training methods against a baseline using plain supervised learning. We also compared the values given by our metric  $\overline{\alpha_{\Delta x}}$  against values given by the metric proposed by Etmann et al. (2019), to which we refer as  $\overline{\alpha_x}$ . We adapted the metric, adding a normalization by  $\|x\|_2$  to change the range of values to  $[0, 1]$ , to allow a comparison with  $\alpha_{\Delta x}$ . The metric was modified as

$$\overline{\alpha_x} = \int P(x) \frac{|\langle x, \nabla \text{logit}(x)_{m(x)} \rangle|}{\|x\|_2 \|\nabla \text{logit}(x)_{m(x)}\|_2} dx. \quad (18)$$

All experiments were performed five times. We report the average resulting values and their standard deviations. Section A.1 of the Supplementary Material presents details about the experimental setup.

#### 3.1. Datasets

We performed evaluations on six datasets, two of which were synthetic datasets for which we could define the correct  $\Delta x$ . For the *Spheres* dataset, defined in Section 2.1, samples were always drawn randomly at runtime from a standard Gaussian distribution and normalized to the radius of the respective class. The correct  $\Delta x$  was calculated by

$$\Delta x = \begin{cases} 0.3 x, & \text{if } \|x\| = 1 \\ -0.3 \frac{x}{1.3}, & \text{if } \|x\| = 1.3 \end{cases} \quad (19)$$

We created another synthetic dataset, to which we refer as *Squares*, composed of images with  $224 \times 224$  pixels of centered squares with sides of 142 or 88 pixels. To make the images unique, spatially smoothed Gaussian noise was randomly sampled for each image and added to it. The direction of alignment  $\Delta x$  for this dataset was calculated using the subtraction of noiseless images from each class.

To evaluate with more complex datasets, we used the MNIST dataset (Lecun et al., 1998), containing handwritten digits, the CIFAR-10 dataset (Krizhevsky, 2009), containing low-resolution natural images, and a binary chest x-ray (CXR) dataset (Schroeder et al., 2020), to which we refer as

Table 1. Examples of measures for generated  $\widehat{\Delta x}$  for the *Spheres* datasets, for two random samples.

CLASS	$\ x\ _2$	$\ \widehat{\Delta x}\ _2$	$\ \widehat{x}'\ _2$	$\ x'\ _2$	$\text{sim}(\Delta x, \widehat{\Delta x})$
-1	1.0	.307	1.27	1.3	.858
1	1.3	.360	0.99	1.0	.898

*COPD*. For the MNIST and CIFAR-10 datasets, a fixed set of 10% of the training set was used for validation. To enable the comparison of the method in a multiclass setting with a corresponding binary setting, we also tested the method with a binary MNIST dataset selecting only two similar digits, 3 and 5, to which we refer as MNIST-3/5. The *COPD* dataset contained posterior-anterior (PA) CXRs labeled for chronic obstructive pulmonary disease (COPD) using pulmonary function tests (PFTs) (Johnson & Theurer, 2014) and was adopted under an approved Institutional Review Board (IRB)<sup>3</sup>. The intensity range of all image datasets was adjusted to  $[-1, 1]$ . For *COPD* and MNIST-3/5, the method presented in Section 2.3.1 was used to estimate  $\Delta x$ , while for MNIST and CIFAR-10, the method presented in Section 2.3.2 was used. More details about the datasets are given in the Supplementary Material, and example images can be seen in Figure 4 and Figure 5.

#### 3.2. Validating the estimation of $\Delta x$

To validate the direct method for estimating  $\Delta x$ , we applied it to both datasets for which we know the correct  $\Delta x$  and measured the alignment between  $\Delta x$  and  $\widehat{\Delta x}$ . We found that, for the *Spheres* dataset,  $\text{sim}(\Delta x, \widehat{\Delta x}) = 0.874 \pm 0.019$ , and, for the *Squares* dataset,  $\text{sim}(\Delta x, \widehat{\Delta x}) = 0.893 \pm 0.058$ , demonstrating close alignment. Table 1 shows examples of results for the *Spheres* dataset. Figure 4 shows examples of generated  $\widehat{\Delta x}$ . The generated  $\widehat{\Delta x}$  were similar to the expected  $\Delta x$  for the *Spheres* and the *Squares* datasets. For the *COPD* dataset,  $\widehat{\Delta x}$  had small norms, with changes mainly around the diaphragms and the upper lungs. Diaphragm shape and position are used as COPD evidence in CXR (Foster Jr et al., 1993). The small norms are likely due to the continuous characteristic of disease severity, which leads to the support of both classes being on the same manifold. Furthermore, most samples had PFT values near the threshold between classes.

For the indirect method for estimating  $\Delta x$ , the chosen cGAN algorithm produced visually good results for the MNIST dataset without any changes to the hyperparameters used for CIFAR-10. We did not apply the method to the *Spheres* dataset because of incompatibilities with the chosen cGAN. To quantitatively validate the indirect

<sup>2</sup>Code is available at <https://github.com/ricbl/gradient-direction-of-robust-models>

<sup>3</sup>IRB\_00104019, PI: Schroeder MD

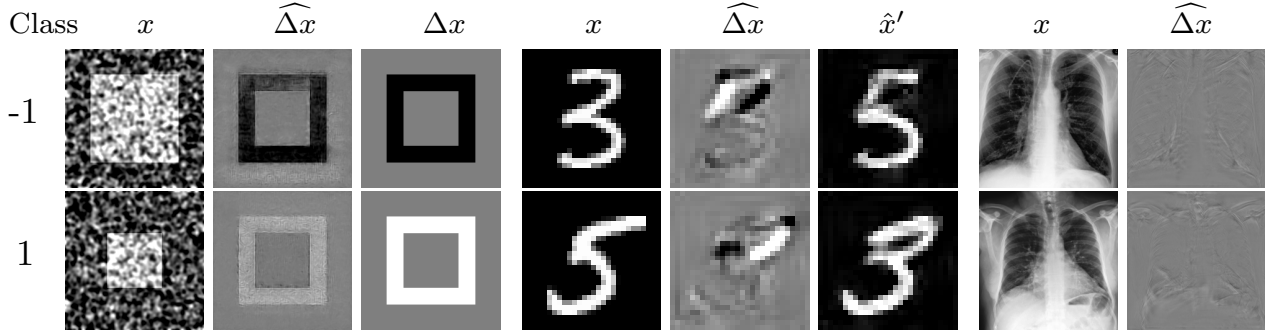


Figure 4. Results of the generated  $\widehat{\Delta x}$  through the direct method for random samples in the image datasets. The  $x'$  column is suppressed for the *COPD* dataset because of its resemblance to  $x$ .

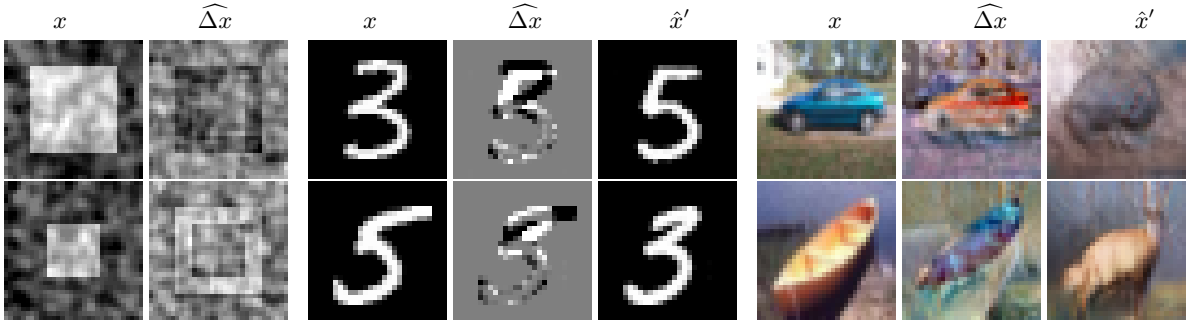


Figure 5. Results of the generated  $\widehat{\Delta x}$  through the indirect method for random samples in the image datasets. The classes for the CIFAR-10 dataset were chosen at random, and the images represent a transition from car to frog and from boat to deer.

method, we applied it to a version of the *Squares* dataset adapted to the capabilities of the chosen cGAN, *Squares32*, for which images had size  $32 \times 32$ , finding an alignment of  $\text{sim}(\Delta x, \widehat{\Delta x}) = 0.661 \pm 0.070$ . This alignment is good but smaller than the alignments found with the direct method. Visually, we found a worse representation of the variability in the background of images for this method when compared to the method proposed in Section 2.3.1, which only needs to generate the differences between classes, adopting the background from the original image. Examples of generated images can be seen in Figure 5 and Section A.4 of the Supplementary Material. A comparison between the generated images for MNIST-3/5 and MNIST showed that the indirect method generates sharper and slightly more distant images. For the CIFAR-10 dataset, generated images resembled the destination class in most cases but failed more often with some destination classes, such as airplanes, and with images containing certain types of scenes, such as white backgrounds. The generated images for MNIST almost always resembled the destination class.

### 3.3. Alignment and robustness

For the robustness metric, we report the estimated point  $\epsilon_{50\%}$  where 50% of test examples are incorrectly classified after applying PGD attack with varying values of  $\epsilon$ . We report a single value instead of the usual curve of accuracy as a function of  $\epsilon$  to have a more objective evaluation. We used accuracy as the basis of the metric to be comparable to the style of reporting in the literature. The defined  $\epsilon_{50\%}$  is equivalent to considering misclassified inputs to have  $\rho(x) = 0$  and calculating the median of the estimated robustness, which has been used to evaluate the baseline metric  $\overline{\alpha_x}$  (Etmann et al., 2019). In addition to using PGD with  $p = \infty$ , we calculated the robustness of the models against  $L^2$ -constrained PGD attacks, with an adapted step  $\eta_{L^2} = \eta_{L^\infty} \times \sqrt{n}$ , where  $n$  is the dimensionality of the data, and against the Square Attack (Andriushchenko et al., 2020), an iterative black-box attack. Since the Square Attack is formulated for images, we adapt it to the *Spheres* dataset by reshaping its 500-feature vectors to a  $20 \times 25$  image. We used the black-box attack to evaluate if any defenses were causing gradient obfuscation (Athalye et al., 2018). For the MNIST, MNIST-3/5, CIFAR-10, and the *COPD* datasets,

Table 2. Results for robustness, alignments, and accuracy after training using a plain supervised training baseline (B), alignment penalty ( $L_\alpha$ ), and adversarial training with PGD (P) for 6 datasets: *Spheres* (S), *Squares* (Q), MNIST-3/5 ( $\mu$ ), *COPD* (X), MNIST (M), CIFAR-10 (C). Attacks employed to calculate robustness include PGD (Madry et al., 2018), with two types of norms, and the black-box Square Attack (Andriushchenko et al., 2020) (BIBox).

SETUP	ACCURACY (%)	$\epsilon_{50\%}$ PGD $_{p=\infty}$	$\epsilon_{50\%}$ PGD $_{p=2}$	$\epsilon_{50\%}$ BLBOX $_{p=\infty}$	$\overline{\alpha_{\Delta x}}$ (OURS)	$\overline{\alpha_x}$
S-B	99.4 $\pm$ 0.8	0.0058 $\pm$ .0001	.099 $\pm$ .009	0.0063 $\pm$ .0004	.659 $\pm$ .028	.659 $\pm$ .028
S- $L_\alpha$	100. $\pm$ 0.0	0.0076 $\pm$ .0002	.133 $\pm$ .001	0.0083 $\pm$ .0003	.886 $\pm$ .002	.886 $\pm$ .002
S-P	100. $\pm$ 0.0	0.0073 $\pm$ .0001	.126 $\pm$ .002	0.0080 $\pm$ .0001	.851 $\pm$ .001	.851 $\pm$ .001
Q-B	100. $\pm$ 0.0	0.031 $\pm$ .008	16.5 $\pm$ 1.6	0.170 $\pm$ .041	.026 $\pm$ .007	.022 $\pm$ .006
Q- $L_\alpha$	100. $\pm$ 0.0	0.435 $\pm$ .061	61.9 $\pm$ 5.4	0.405 $\pm$ .001	.926 $\pm$ .004	.357 $\pm$ .009
Q-P	100. $\pm$ 0.0	0.501 $\pm$ .030	61.3 $\pm$ 2.0	0.337 $\pm$ .011	.222 $\pm$ .042	.151 $\pm$ .051
$\mu$ -B	99.3 $\pm$ 0.4	0.198 $\pm$ .012	2.36 $\pm$ .11	0.232 $\pm$ .010	.171 $\pm$ .029	.013 $\pm$ .003
$\mu$ - $L_\alpha$	99.5 $\pm$ 0.5	0.357 $\pm$ .011	3.88 $\pm$ .08	0.351 $\pm$ .009	.678 $\pm$ .078	.196 $\pm$ .010
$\mu$ -P	99.5 $\pm$ 0.2	0.547 $\pm$ .007	4.20 $\pm$ .15	0.495 $\pm$ .005	.345 $\pm$ .018	.040 $\pm$ .032
X-B	66.3 $\pm$ 1.5	0.006 $\pm$ .0021	0.73 $\pm$ .33	0.021 $\pm$ .0063	.016 $\pm$ .005	.002 $\pm$ .0003
X- $L_\alpha$	64.2 $\pm$ 5.4	0.020 $\pm$ .0047	2.91 $\pm$ .65	0.028 $\pm$ .0074	.163 $\pm$ .009	.064 $\pm$ .019
X-P	64.7 $\pm$ 2.7	0.063 $\pm$ .0294	4.97 $\pm$ 2.4	0.072 $\pm$ .0324	.081 $\pm$ .007	.023 $\pm$ .013
M-B	99.2 $\pm$ 0.2	0.171 $\pm$ .004	2.19 $\pm$ .06	0.188 $\pm$ 0.003	.075 $\pm$ .006	.038 $\pm$ .005
M- $L_\alpha$	99.2 $\pm$ 0.1	0.325 $\pm$ .009	3.55 $\pm$ .06	0.308 $\pm$ 0.007	.592 $\pm$ .009	.320 $\pm$ .009
M-P	99.4 $\pm$ 0.0	0.554 $\pm$ .007	4.32 $\pm$ .07	0.489 $\pm$ 0.001	.181 $\pm$ .012	.043 $\pm$ .008
C-B	84.0 $\pm$ 0.2	0.008 $\pm$ .0003	.23 $\pm$ .121	0.008 $\pm$ 0.005	.008 $\pm$ .003	.008 $\pm$ .000
C- $L_\alpha$	81.1 $\pm$ 0.6	0.012 $\pm$ .0006	.44 $\pm$ .023	0.016 $\pm$ 0.001	.025 $\pm$ .002	.020 $\pm$ .002
C-P	82.6 $\pm$ 0.1	0.023 $\pm$ .0001	.77 $\pm$ .003	0.028 $\pm$ 0.000	.041 $\pm$ .001	.031 $\pm$ .001

training with alignment penalty as defined in (9) employed a distinct  $G$  for each run, and, for calculating the reported  $\overline{\alpha_{\Delta x}}$ , a different  $G$  than the one used for training. We used the correct  $\Delta x$  to calculate  $L_\alpha$  and  $\overline{\alpha_{\Delta x}}$  for the *Spheres* and *Squares* datasets. Table 2 presents results for robustness and alignment. Graphs of accuracy as a function of  $\epsilon$  are given in Section A.7 in the Supplementary Material.

The alignment  $\overline{\alpha_{\Delta x}}$  increased for all PGD-trained models (rows P) when compared to the baseline (rows B). Similarly, the robustness of all models trained with the  $L_\alpha$  penalty increased when compared to the baseline (rows B). These results show that alignment  $\overline{\alpha_{\Delta x}}$  and robustness are closely related, and one is a consequence of the other. Theoretically, for the *Spheres* dataset,  $\rho_x / \overline{\alpha_{\Delta x}} = 0.15$  when  $p = 2$ . This value is very close to the ratios of corresponding values in Table 2, which lie between 0.148 and 0.151.

In Table 2, models trained using PGD exhibited the strongest signs of gradient obfuscation, highlighted by the black-box attack (column  $\epsilon_{50\%}$ , BLBOX $_{p=\infty}$ ) being considerably more potent than the PGD attack (column  $\epsilon_{50\%}$ , PGD $_{p=\infty}$ ) for some datasets. Section A.7 in the Supplementary Material provides an analysis of gradient obfuscation using the graphs of accuracy as a function of perturbation norm.

Except for the *Spheres* dataset, where our proposed alignment metrics  $\alpha_{\Delta x}$  mathematically reduces to the alignment metric  $\alpha_x$  (Etmann et al., 2019), our metric  $\overline{\alpha_{\Delta x}}$  was larger

than  $\overline{\alpha_x}$  in all cases, demonstrating that robust models are more closely aligned with  $\Delta x$  than with  $x$ . It is also worth noting that  $\overline{\alpha_{\Delta x}}$  employs the direction to which the gradient is pointing, providing more information than the  $\overline{\alpha_x}$  metric, which has an absolute value in its numerator. Furthermore, in addition to a different alignment direction ( $\Delta x$ ), our proposed metric proposes a different definition of what is aligning to that direction,  $\nabla_{\logit(x)_{\tilde{e}(x)} - \logit(x)_y}$  against  $\nabla_{\logit(x)_{m(x)}}$  for the baseline metric  $\overline{\alpha_x}$ . The metric we reported corresponds to the highest alignment for the baseline metric considering several possible methods for calculating the input gradient, as shown in Section A.5 in the Supplementary Material.

For most of the datasets, even though the penalty alignment training (rows  $L_\alpha$ ) had the closest alignment (columns  $\overline{\alpha_{\Delta x}}$  and  $\overline{\alpha_x}$ ), PGD (rows P) had the highest robustness when  $p = \infty$  (column  $\epsilon_{50\%}$ , PGD $_{p=\infty}$ ). PGD likely not only aligns the gradient but also improves robustness in other ways, such as possibly providing a denser sampling of inputs, especially in critical regions, and making the model more locally linear (Qin et al., 2019). When setting the training method to PGD-training, with varying values of  $\epsilon$ , both metrics showed a good Pearson correlation with robustness, as seen in Table 3. Our metric showed a better correlation for most datasets. Graphs of the data used to calculate these correlations are provided in Section A.6 of the Supplementary Material.



Table 3. Pearson correlation between alignment metrics and robustness against PGD attack ( $\epsilon_{50\%}$ ,  $\text{PGD}_{p=\infty}$ ) for our proposed metric and the baseline metric  $\overline{\alpha}_x$  (Etman et al., 2019), with PGD-training as a constant training method. For each dataset, five models were trained for each of 6 or 7 values of  $\epsilon$ .

DATASET	$\overline{\alpha}_{\Delta x}$ (OURS)	$\overline{\alpha}_x$
<i>Spheres</i>	.818	.818
<i>Squares</i>	.883	.870
MNIST-3/5	.861	.591
<i>COPD</i>	.280	.656
MNIST	.897	.185
CIFAR-10	.996	.994

When comparing results between MNIST and MNIST-3/5, robustness was similar for the  $L_\alpha$  training method, but  $\overline{\alpha}_{\Delta x}$  was lower for PGD-training for MNIST. The  $\overline{\alpha}_{\Delta x}$  achieved for the CIFAR-10 dataset showed that the alignment with  $\Delta x$  is sometimes easier to learn with PGD than with  $L_\alpha$ .

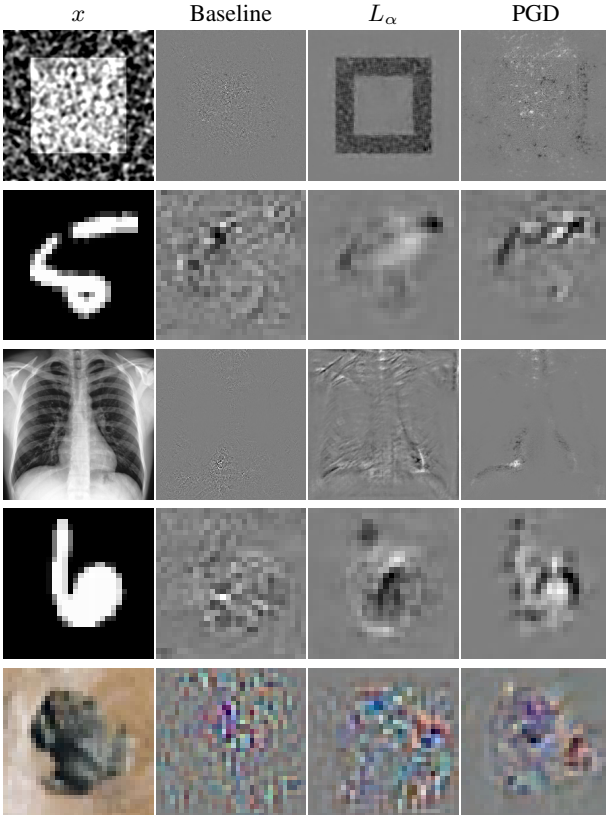


Figure 6. Examples of the calculated  $\nabla_{\ell(x)}$  for all the training methods for the datasets, from top to bottom: *Squares*, MNIST-3/5, *COPD*, MNIST, CIFAR-10.

### 3.4. Validity of local linearity assumption

Figure 7 qualitatively surveys the validity of the equations from Lemma 1 as an approximation of a model’s robustness. For a minority of the datasets and methods, the approximated robustness is very similar to the robustness. The fact that the approximation from Lemma 1 does not hold perfectly may be one of the reasons for an imperfect correlation between alignment and robustness.

### 3.5. Qualitative analysis of the changes to the input gradient

Figure 6 shows  $\nabla_{\ell(x)}$  for random images in each dataset for all three training methods. The calculated  $\nabla_{\ell(x)}$  are noisier for the baseline and smoother for models trained with  $L_\alpha$ , whereas PGD-trained models have an intermediate amount of noise and are more localized. Part of the differences in the  $\nabla_{\ell(x)}$  produced for the MNIST dataset for the  $L_\alpha$  and PGD methods is caused by the different  $\tilde{c}(x)$  in each case. For this specific sample  $\tilde{c}(x) = 0$  for the model trained with  $L_\alpha$  and  $\tilde{c}(x) = 4$  for the model trained with PGD.

## 4. Conclusion

We proposed a novel alignment direction for the gradient of robust models as the vector pointing to the closest example of the support of the closest inaccurate class. We validated the proposed direction theoretically and showed experimentally that alignment increases with PGD training and that robustness increases with alignment enforcement. Trained models also showed a closer alignment with the proposed metric than with another metric definition. The metric was not directly predictive of robustness since models with the strongest alignment were not always the most robust. This finding is possibly a result of the violation of the strong assumptions of the theoretical analysis. It also highlights the possibility of PGD increasing robustness by means other than gradient alignment. When comparing models trained with PGD with varying levels of robustness, the proposed metric correlated better with the robustness than the baseline metric for most datasets. Finally, we expand our fundamental understanding of adversarial defenses, benefiting future analyses of model robustness.

## Acknowledgements

Copyediting support was provided by Christine Pickett. Funding: This work was supported by the National Institute Of Biomedical Imaging And Bioengineering of the National Institutes of Health [grant numbers R21EB028367]. The funding source had no other involvement in the study.

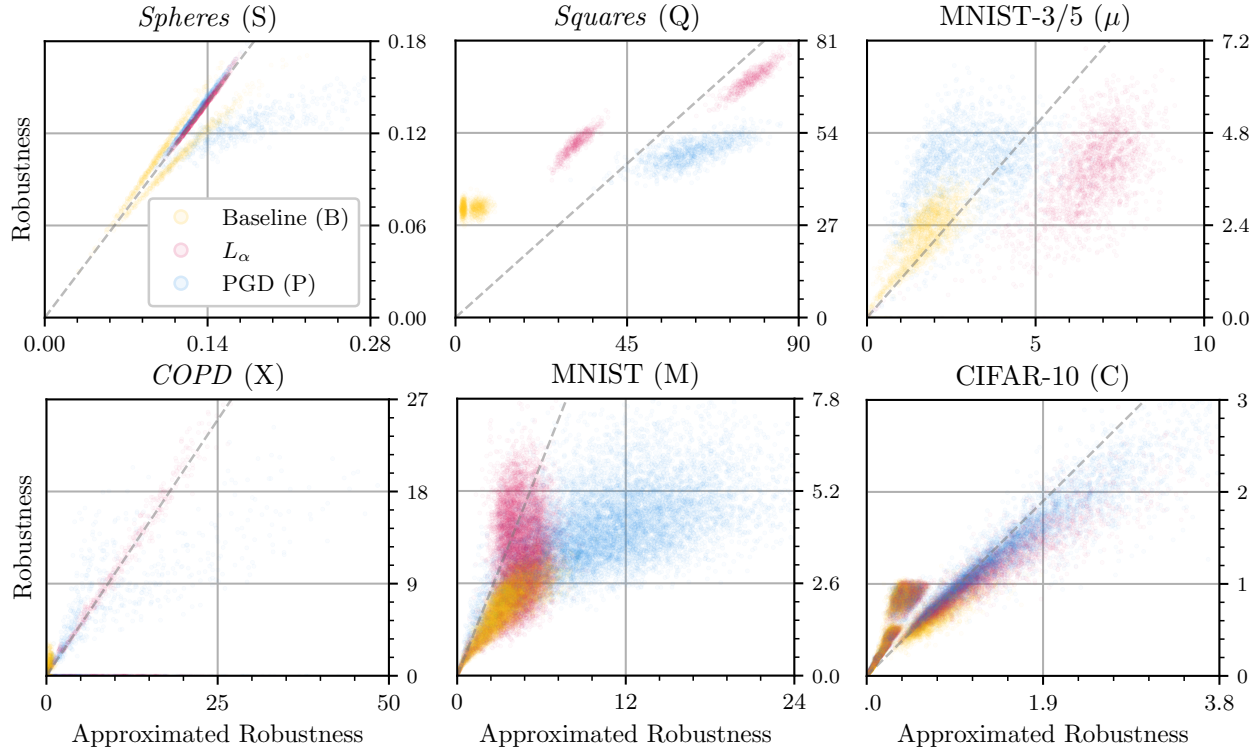


Figure 7. Robustness against  $L^2$  Carlini-Wagner attack (Carlini & Wagner, 2017a) as a function of the approximated robustness given by Lemma 1, for 6 datasets and 3 training methods. Each marker represents one test set example. The dashed diagonal gray line represents the identity function. Models were selected randomly from the 5 trained models for each training setup.

## References

- Abadi, M., Agarwal, A., Barham, P., Brevdo, E., Chen, Z., Citro, C., Corrado, G. S., Davis, A., Dean, J., Devin, M., Ghemawat, S., Goodfellow, I. J., Harp, A., Irving, G., Isard, M., Jia, Y., Józefowicz, R., Kaiser, L., Kudlur, M., Levenberg, J., Mané, D., Monga, R., Moore, S., Murray, D. G., Olah, C., Schuster, M., Shlens, J., Steiner, B., Sutskever, I., Talwar, K., Tucker, P. A., Vanhoucke, V., Vasudevan, V., Viégas, F. B., Vinyals, O., Warden, P., Wattenberg, M., Wicke, M., Yu, Y., and Zheng, X. Tensorflow: Large-scale machine learning on heterogeneous distributed systems. *CoRR*, abs/1603.04467, 2016. URL <http://arxiv.org/abs/1603.04467>.
- Andriushchenko, M., Croce, F., Flammarion, N., and Hein, M. Square attack: A query-efficient black-box adversarial attack via random search. In Vedaldi, A., Bischof, H., Brox, T., and Frahm, J. (eds.), *Computer Vision - ECCV 2020 - 16th European Conference, Glasgow, UK, August 23-28, 2020, Proceedings, Part XXIII*, volume 12368 of *Lecture Notes in Computer Science*, pp. 484–501. Springer, 2020. doi: 10.1007/978-3-030-58592-1\_29. URL [https://doi.org/10.1007/978-3-030-58592-1\\_29](https://doi.org/10.1007/978-3-030-58592-1_29).
- Athalye, A., Carlini, N., and Wagner, D. A. Obfuscated gradients give a false sense of security: Circumventing defenses to adversarial examples. In Dy, J. G. and Krause, A. (eds.), *Proceedings of the 35th International Conference on Machine Learning, ICML 2018, Stockholmsmässan, Stockholm, Sweden, July 10-15, 2018*, volume 80 of *Proceedings of Machine Learning Research*, pp. 274–283. PMLR, 2018. URL <http://proceedings.mlr.press/v80/athalye18a.html>.
- Boopathy, A., Liu, S., Zhang, G., Liu, C., Chen, P., Chang, S., and Daniel, L. Proper network interpretability helps adversarial robustness in classification. In *Proceedings of the 37th International Conference on Machine Learning, ICML 2020, 13-18 July 2020, Virtual Event*, volume 119 of *Proceedings of Machine Learning Research*, pp. 1014–1023. PMLR, 2020. URL <http://proceedings.mlr.press/v119/boopathy20a.html>.
- Carlini, N. and Wagner, D. A. Towards evaluating the robustness of neural networks. In *2017 IEEE Symposium on Security and Privacy, SP 2017, San Jose, CA, USA, May 22-26, 2017*, pp. 39–57. IEEE Com-

- puter Society, 2017a. doi: 10.1109/SP.2017.49. URL <https://doi.org/10.1109/SP.2017.49>.
- Carlini, N. and Wagner, D. A. Adversarial examples are not easily detected: Bypassing ten detection methods. In Thuraishingham, B. M., Biggio, B., Freeman, D. M., Miller, B., and Sinha, A. (eds.), *Proceedings of the 10th ACM Workshop on Artificial Intelligence and Security, AISec@CCS 2017, Dallas, TX, USA, November 3, 2017*, pp. 3–14. ACM, 2017b. doi: 10.1145/3128572.3140444. URL <https://doi.org/10.1145/3128572.3140444>.
- Carlini, N., Katz, G., Barrett, C. W., and Dill, D. L. Ground-truth adversarial examples. *CoRR*, abs/1709.10207, 2017. URL <http://arxiv.org/abs/1709.10207>.
- Caswell, T. A., Droettboom, M., Lee, A., Hunter, J., de Andrade, E. S., Firing, E., Hoffmann, T., Klymak, J., Stansby, D., Varoquaux, N., Nielsen, J. H., Root, B., May, R., Elson, P., Seppänen, J. K., Dale, D., Lee, J.-J., McDougall, D., Straw, A., Hobson, P., Gohlke, C., Yu, T. S., Ma, E., Vincent, A. F., Silvester, S., Moad, C., Kniazev, N., hannah, Ernest, E., and Ivanov, P. matplotlib/matplotlib: Rel: v3.3.2, September 2020. URL <https://doi.org/10.5281/zenodo.4030140>.
- Chan, A., Tay, Y., and Ong, Y. What it thinks is important is important: Robustness transfers through input gradients. In *2020 IEEE/CVF Conference on Computer Vision and Pattern Recognition, CVPR 2020, Seattle, WA, USA, June 13-19, 2020*, pp. 329–338. IEEE, 2020a. doi: 10.1109/CVPR42600.2020.00041. URL <https://doi.org/10.1109/CVPR42600.2020.00041>.
- Chan, A., Tay, Y., Ong, Y., and Fu, J. Jacobian adversarially regularized networks for robustness. In *8th International Conference on Learning Representations, ICLR 2020, Addis Ababa, Ethiopia, April 26-30, 2020*. OpenReview.net, 2020b. URL <https://openreview.net/forum?id=Hke0VlrKPS>.
- Collette, A., Caswell, T. A., Tocknell, J., Kluyver, T., Dale, D., Scopatz, A., Jelenak, A., Valls, V., Pedersen, U. K., Raspaud, M., jakirkham, Parsons, A., jialin, Chan, L., Paramonov, A., Hole, L., Feng, Y., Johnson, S. R., Brucher, M., Teichmann, M., Vaillant, G. A., de Buyl, P., Hinsén, K., Huebl, A., VINCENT, T., Dietz, M., Rathgeber, F., Billington, C., Kieffer, J., and Wright, G. h5py/h5py: 2.10.0, September 2019. URL <https://doi.org/10.5281/zenodo.3401726>.
- Ding, G. W., Wang, L., and Jin, X. AdverTorch v0.1: An adversarial robustness toolbox based on pytorch. *arXiv preprint arXiv:1902.07623*, 2019.
- Etmann, C., Lunz, S., Maass, P., and Schönlieb, C. On the connection between adversarial robustness and saliency map interpretability. In Chaudhuri, K. and Salakhutdinov, R. (eds.), *Proceedings of the 36th International Conference on Machine Learning, ICML 2019, 9-15 June 2019, Long Beach, California, USA*, volume 97 of *Proceedings of Machine Learning Research*, pp. 1823–1832. PMLR, 2019. URL <http://proceedings.mlr.press/v97/etmann19a.html>.
- Finlay, C. and Oberman, A. M. Scaleable input gradient regularization for adversarial robustness. *Machine Learning with Applications*, 3:100017, 2021. ISSN 2666-8270. doi: <https://doi.org/10.1016/j.mlwa.2020.100017>. URL <http://www.sciencedirect.com/science/article/pii/S2666827020300177>.
- Foster Jr, W., Gimenez, E., Roubidoux, M., Sherrier, R., Shannon, R., Roggli, V., and Pratt, P. The emphysemas: radiologic-pathologic correlations. *Radiographics*, 13(2): 311–328, 1993.
- Galloway, A., Golubeva, A., Tanay, T., Moussa, M., and Taylor, G. W. Batch normalization is a cause of adversarial vulnerability. *CoRR*, abs/1905.02161, 2019. URL <http://arxiv.org/abs/1905.02161>.
- Gilmer, J., Metz, L., Faghri, F., Schoenholz, S. S., Raghu, M., Wattenberg, M., and Goodfellow, I. J. Adversarial spheres. In *6th International Conference on Learning Representations, ICLR 2018, Vancouver, BC, Canada, April 30 - May 3, 2018, Workshop Track Proceedings*. OpenReview.net, 2018. URL <https://openreview.net/forum?id=SkthlLkPf>.
- Goodfellow, I. J., Pouget-Abadie, J., Mirza, M., Xu, B., Warde-Farley, D., Ozair, S., Courville, A. C., and Bengio, Y. Generative adversarial nets. In Ghahramani, Z., Welling, M., Cortes, C., Lawrence, N. D., and Weinberger, K. Q. (eds.), *Advances in Neural Information Processing Systems 27: Annual Conference on Neural Information Processing Systems 2014, December 8-13 2014, Montreal, Quebec, Canada*, pp. 2672–2680, 2014. URL <http://papers.nips.cc/paper/5423-generative-adversarial-nets>.
- Goodfellow, I. J., Shlens, J., and Szegedy, C. Explaining and harnessing adversarial examples. In Bengio, Y. and LeCun, Y. (eds.), *3rd International Conference on Learning Representations, ICLR 2015, San Diego, CA, USA, May 7-9, 2015, Conference Track Proceedings*, 2015. URL <http://arxiv.org/abs/1412.6572>.
- Guo, C., Rana, M., Cissé, M., and van der Maaten, L. Countering adversarial images using input transformations. In *6th International Conference on Learning Representations, ICLR 2018, Vancouver, BC, Canada, April 30 -*

- May 3, 2018, *Conference Track Proceedings*. OpenReview.net, 2018. URL <https://openreview.net/forum?id=SyJ7ClWCb>.
- Harris, C. R., Millman, K. J., van der Walt, S. J., Gommers, R., Virtanen, P., Cournapeau, D., Wieser, E., Taylor, J., Berg, S., Smith, N. J., Kern, R., Picus, M., Hoyer, S., van Kerkwijk, M. H., Brett, M., Haldane, A., del Río, J. F., Wiebe, M., Peterson, P., Gérard-Marchant, P., Sheppard, K., Reddy, T., Weckesser, W., Abbasi, H., Gohlke, C., and Oliphant, T. E. Array programming with NumPy. *Nature*, 585(7825):357–362, September 2020. doi: 10.1038/s41586-020-2649-2. URL <https://doi.org/10.1038/s41586-020-2649-2>.
- He, K., Zhang, X., Ren, S., and Sun, J. Delving deep into rectifiers: Surpassing human-level performance on ImageNet classification. In *2015 IEEE International Conference on Computer Vision, ICCV 2015, Santiago, Chile, December 7-13, 2015*, pp. 1026–1034. IEEE Computer Society, 2015. doi: 10.1109/ICCV.2015.123. URL <https://doi.org/10.1109/ICCV.2015.123>.
- He, K., Zhang, X., Ren, S., and Sun, J. Deep residual learning for image recognition. In *2016 IEEE Conference on Computer Vision and Pattern Recognition, CVPR 2016, Las Vegas, NV, USA, June 27-30, 2016*, pp. 770–778. IEEE Computer Society, 2016. doi: 10.1109/CVPR.2016.90. URL <https://doi.org/10.1109/CVPR.2016.90>.
- Hein, M. and Andriushchenko, M. Formal guarantees on the robustness of a classifier against adversarial manipulation. In Guyon, I., von Luxburg, U., Bengio, S., Wallach, H. M., Fergus, R., Vishwanathan, S. V. N., and Garnett, R. (eds.), *Advances in Neural Information Processing Systems 30: Annual Conference on Neural Information Processing Systems 2017, 4-9 December 2017, Long Beach, CA, USA*, pp. 2266–2276, 2017.
- Helland, J. and VanHoudnos, N. M. On the human-recognizability phenomenon of adversarially trained deep image classifiers. In *JSM Proceedings, Statistical Computing Section*. Alexandria, VA: American Statistical Association, pp. 1121–1131, 2020. URL <https://arxiv.org/abs/2101.05219>.
- Hunter, J. D. Matplotlib: A 2d graphics environment. *Computing in Science & Engineering*, 9(3):90–95, 2007. doi: 10.1109/MCSE.2007.55.
- Ilyas, A., Santurkar, S., Tsipras, D., Engstrom, L., Tran, B., and Madry, A. Adversarial examples are not bugs, they are features. In Wallach, H. M., Larochelle, H., Beygelzimer, A., d’Alché-Buc, F., Fox, E. B., and Garnett, R. (eds.), *Advances in Neural Information Processing Systems 32: Annual Conference on Neural Information Processing Systems 2019, NeurIPS 2019, 8-14 December 2019, Vancouver, BC, Canada*, pp. 125–136, 2019. URL <http://papers.nips.cc/paper/8307-adversarial-examples-are-not-bugs-they-are-features>.
- Ioffe, S. and Szegedy, C. Batch normalization: Accelerating deep network training by reducing internal covariate shift. In Bach, F. R. and Blei, D. M. (eds.), *Proceedings of the 32nd International Conference on Machine Learning, ICML 2015, Lille, France, 6-11 July 2015*, volume 37 of *JMLR Workshop and Conference Proceedings*, pp. 448–456. JMLR.org, 2015. URL <http://proceedings.mlr.press/v37/ioffe15.html>.
- Jakobovitz, D. and Giryes, R. Improving DNN robustness to adversarial attacks using Jacobian regularization. In Ferrari, V., Hebert, M., Sminchisescu, C., and Weiss, Y. (eds.), *Computer Vision - ECCV 2018 - 15th European Conference, Munich, Germany, September 8-14, 2018, Proceedings, Part XII*, volume 11216 of *Lecture Notes in Computer Science*, pp. 525–541. Springer, 2018. doi: 10.1007/978-3-030-01258-8\_32. URL [https://doi.org/10.1007/978-3-030-01258-8\\_32](https://doi.org/10.1007/978-3-030-01258-8_32).
- Johnson, J. D. and Theurer, W. M. A stepwise approach to the interpretation of pulmonary function tests. *American family physician*, 89 5:359–66, 2014.
- Kaur, S., Cohen, J., and Lipton, Z. C. Are perceptually-aligned gradients a general property of robust classifiers? *CoRR*, abs/1910.08640, 2019. URL <http://arxiv.org/abs/1910.08640>.
- Kavalerov, I., Czaja, W., and Chellappa, R. A study of quality and diversity in k+1 GANs. In *“I Can’t Believe It’s Not Better!” NeurIPS 2020 workshop*, 2020. URL <https://openreview.net/forum?id=kBk6w-oJ9jq>.
- Kingma, D. P. and Ba, J. Adam: A method for stochastic optimization. In Bengio, Y. and LeCun, Y. (eds.), *3rd International Conference on Learning Representations, ICLR 2015, San Diego, CA, USA, May 7-9, 2015, Conference Track Proceedings*, 2015. URL <http://arxiv.org/abs/1412.6980>.
- Krizhevsky, A. Learning multiple layers of features from tiny images. Technical report, 2009.
- Lanfredi, R. B., Schroeder, J. D., Vachet, C., and Tadziden, T. Adversarial regression training for visualizing the progression of chronic obstructive pulmonary disease with chest x-rays. In Shen, D., Liu, T., Peters, T. M., Staib, L. H., Essert, C., Zhou, S., Yap, P., and Khan, A. (eds.), *Medical Image Computing and Computer Assisted Intervention - MICCAI 2019 - 22nd International Conference, Shenzhen, China, October 13-17,*



- 2019, *Proceedings, Part VI*, volume 11769 of *Lecture Notes in Computer Science*, pp. 685–693. Springer, 2019. doi: 10.1007/978-3-030-32226-7\\_76. URL <https://doi.org/10.1007/978-3-030-32226-7-76>.
- Lecun, Y., Bottou, L., Bengio, Y., and Haffner, P. Gradient-based learning applied to document recognition. *Proceedings of the IEEE*, 86(11):2278–2324, 1998.
- Lyu, C., Huang, K., and Liang, H. A unified gradient regularization family for adversarial examples. In Agarwal, C. C., Zhou, Z., Tuzhilin, A., Xiong, H., and Wu, X. (eds.), *2015 IEEE International Conference on Data Mining, ICDM 2015, Atlantic City, NJ, USA, November 14-17, 2015*, pp. 301–309. IEEE Computer Society, 2015. doi: 10.1109/ICDM.2015.84. URL <https://doi.org/10.1109/ICDM.2015.84>.
- Madry, A., Makelov, A., Schmidt, L., Tsipras, D., and Vladu, A. Towards deep learning models resistant to adversarial attacks. In *6th International Conference on Learning Representations, ICLR 2018, Vancouver, BC, Canada, April 30 - May 3, 2018, Conference Track Proceedings*. OpenReview.net, 2018. URL <https://openreview.net/forum?id=rJzIBfZAb>.
- Marcel, S. and Rodriguez, Y. Torchvision the machine-vision package of torch. *Proceedings of the 18th ACM international conference on Multimedia*, 2010.
- Mirza, M. and Osindero, S. Conditional generative adversarial nets. *CoRR*, abs/1411.1784, 2014. URL <http://arxiv.org/abs/1411.1784>.
- Nandy, J., Hsu, W., and Lee, M. Approximate manifold defense against multiple adversarial perturbations. In *2020 International Joint Conference on Neural Networks, IJCNN 2020, Glasgow, United Kingdom, July 19-24, 2020*, pp. 1–8. IEEE, 2020. doi: 10.1109/IJCNN48605.2020.9207312. URL <https://doi.org/10.1109/IJCNN48605.2020.9207312>.
- Noack, A., Ahern, I., Dou, D., and Li, B. An empirical study on the relation between network interpretability and adversarial robustness. *SN Comput. Sci.*, 2(1):32, 2021. doi: 10.1007/s42979-020-00390-x. URL <https://doi.org/10.1007/s42979-020-00390-x>.
- Paszke, A., Gross, S., Massa, F., Lerer, A., Bradbury, J., Chanan, G., Killeen, T., Lin, Z., Gimelshein, N., Antiga, L., Desmaison, A., Köpf, A., Yang, E., DeVito, Z., Raison, M., Tejani, A., Chilamkurthy, S., Steiner, B., Fang, L., Bai, J., and Chintala, S. PyTorch: An imperative style, high-performance deep learning library. In Wallach, H. M., Larochelle, H., Beygelzimer, A., d’Alché-Buc, F., Fox, E. B., and Garnett, R. (eds.), *Advances in Neural Information Processing Systems 32: Annual Conference on Neural Information Processing Systems 2019, NeurIPS 2019, December 8-14, 2019, Vancouver, BC, Canada*, pp. 8024–8035, 2019. URL <https://proceedings.neurips.cc/paper/2019/hash/bdbca288fee7f92f2bfa9f7012727740-Abstract.html>.
- Qin, C., Martens, J., Goyal, S., Krishnan, D., Dvijotham, K., Fawzi, A., De, S., Stanforth, R., and Kohli, P. Adversarial robustness through local linearization. In Wallach, H. M., Larochelle, H., Beygelzimer, A., d’Alché-Buc, F., Fox, E. B., and Garnett, R. (eds.), *Advances in Neural Information Processing Systems 32: Annual Conference on Neural Information Processing Systems 2019, NeurIPS 2019, 8-14 December 2019, Vancouver, BC, Canada*, pp. 13824–13833, 2019. URL <http://papers.nips.cc/paper/9534-adversarial-robustness-through-local-linearization>.
- Reback, J., McKinney, W., jbrockmendel, den Bossche, J. V., Augspurger, T., Cloud, P., gfyong, Hawkins, S., Sinhrks, Roeschke, M., Klein, A., Petersen, T., Tratner, J., She, C., Ayd, W., Naveh, S., Garcia, M., Schendel, J., Hayden, A., Saxton, D., Jancauskas, V., patrick, McMaster, A., Battiston, P., Seabold, S., Dong, K., chris b1, h vetinari, Hoyer, S., and Gorelli, M. pandas-dev/pandas: Pandas 1.2.0, December 2020. URL <https://doi.org/10.5281/zenodo.4394318>.
- Ronneberger, O., Fischer, P., and Brox, T. U-net: Convolutional networks for biomedical image segmentation. In Navab, N., Hornegger, J., III, W. M. W., and Frangi, A. F. (eds.), *Medical Image Computing and Computer-Assisted Intervention - MICCAI 2015 - 18th International Conference Munich, Germany, October 5 - 9, 2015, Proceedings, Part III*, volume 9351 of *Lecture Notes in Computer Science*, pp. 234–241. Springer, 2015. doi: 10.1007/978-3-319-24574-4\\_28. URL <https://doi.org/10.1007/978-3-319-24574-4-28>.
- Ross, A. S. and Doshi-Velez, F. Improving the adversarial robustness and interpretability of deep neural networks by regularizing their input gradients. In McIlraith, S. A. and Weinberger, K. Q. (eds.), *Proceedings of the Thirty-Second AAAI Conference on Artificial Intelligence, (AAAI-18), the 30th innovative Applications of Artificial Intelligence (IAAI-18), and the 8th AAAI Symposium on Educational Advances in Artificial Intelligence (EAAI-18), New Orleans, Louisiana, USA, February 2-7, 2018*, pp. 1660–1669. AAAI Press, 2018. URL <https://www.aaai.org/ocs/index.php/AAAI/AAAI18/paper/view/17337>.

- Samangouei, P., Kabkab, M., and Chellappa, R. Defense-GAN: Protecting classifiers against adversarial attacks using generative models. In *6th International Conference on Learning Representations, ICLR 2018, Vancouver, BC, Canada, April 30 - May 3, 2018, Conference Track Proceedings*. OpenReview.net, 2018. URL <https://openreview.net/forum?id=BkJ3ibb0->.
- Schroeder, J. D., Lanfredi, R. B., Li, T., Chan, J., Vachet, C., Paine III, R., Srikumar, V., and Tasdizen, T. Prediction of obstructive lung disease from chest radiographs via deep learning trained on pulmonary function data. *International Journal of Chronic Obstructive Pulmonary Disease*, 15:3455, 2020.
- Smilkov, D., Thorat, N., Kim, B., Viégas, F. B., and Wattenberg, M. Smoothgrad: removing noise by adding noise. *CoRR*, abs/1706.03825, 2017. URL <http://arxiv.org/abs/1706.03825>.
- Tanay, T. and Griffin, L. D. A boundary tilting perspective on the phenomenon of adversarial examples. *CoRR*, abs/1608.07690, 2016. URL <http://arxiv.org/abs/1608.07690>.
- Tsipras, D., Santurkar, S., Engstrom, L., Turner, A., and Madry, A. Robustness may be at odds with accuracy. In *7th International Conference on Learning Representations, ICLR 2019, New Orleans, LA, USA, May 6-9, 2019*. OpenReview.net, 2019. URL <https://openreview.net/forum?id=SyxAb30cY7>.
- van der Walt, S., Schönberger, J. L., Nunez-Iglesias, J., Boulogne, F., Warner, J. D., Yager, N., Gouillart, E., Yu, T., and the scikit-image contributors. scikit-image: image processing in Python. *PeerJ*, 2:e453, 6 2014. ISSN 2167-8359. doi: 10.7717/peerj.453. URL <https://doi.org/10.7717/peerj.453>.
- Weng, T., Zhang, H., Chen, P., Yi, J., Su, D., Gao, Y., Hsieh, C., and Daniel, L. Evaluating the robustness of neural networks: An extreme value theory approach. In *6th International Conference on Learning Representations, ICLR 2018, Vancouver, BC, Canada, April 30 - May 3, 2018, Conference Track Proceedings*. OpenReview.net, 2018. URL <https://openreview.net/forum?id=BkUHLmZ0b>.
- Wes McKinney. Data Structures for Statistical Computing in Python. In Stéfan van der Walt and Jarrod Millman (eds.), *Proceedings of the 9th Python in Science Conference*, pp. 56 – 61, 2010. doi: 10.25080/Majora-92bf1922-00a.
- Xu, H., Ma, Y., Liu, H., Deb, D., Liu, H., Tang, J., and Jain, A. K. Adversarial attacks and defenses in images, graphs and text: A review. *Int. J. Autom. Comput.*, 17 (2):151–178, 2020. doi: 10.1007/s11633-019-1211-x.
- URL <https://doi.org/10.1007/s11633-019-1211-x>.
- Zhang, H., Yu, Y., Jiao, J., Xing, E. P., Ghaoui, L. E., and Jordan, M. I. Theoretically principled trade-off between robustness and accuracy. In Chaudhuri, K. and Salakhutdinov, R. (eds.), *Proceedings of the 36th International Conference on Machine Learning, ICML 2019, 9-15 June 2019, Long Beach, California, USA*, volume 97 of *Proceedings of Machine Learning Research*, pp. 7472–7482. PMLR, 2019. URL <http://proceedings.mlr.press/v97/zhang19p.html>.

## A. Supplementary Material

### A.1. Experimental setup and dataset details

We used PyTorch (Paszke et al., 2019), torchvision (Marcel & Rodriguez, 2010), advtorch (Ding et al., 2019), NumPy (Harris et al., 2020), pandas (Wes McKinney, 2010; Reback et al., 2020), h5py (Collette et al., 2019), scikit-image (van der Walt et al., 2014), Matplotlib (Hunter, 2007; Caswell et al., 2020) and TensorBoard (Abadi et al., 2016) to build our experiments. For the *Spheres* dataset, we used a 2-hidden layer network, with 1000 neurons per layer and ReLU non-linearity, and a last-layer output of a 500-dimensional vector for the generator and a scalar for the classifiers. For all other datasets, we used a Resnet-18 (He et al., 2016) as the classifier, with weights pre-trained for ImageNet loaded from PyTorch’s torchvision library. PGD attacks, for training and validation, used  $k = 40$ . The Square Attack was used with 5000 queries per attack and 80% as an initial percentage of features to be modified. We used the Adam optimizer (Kingma & Ba, 2015) with a learning rate of  $10^{-4}$ , except for the CIFAR-10 dataset. Hyperparameters were chosen by checking for best robustness given that accuracy with no attack does not drop by more than 4%. The best epoch was chosen by the highest robustness against PGD ( $p = \infty$ ) on the validation set. When there was little or no impact to accuracy, which includes all datasets except the CIFAR-10 dataset, batch normalization (Ioffe & Szegedy, 2015) was turned off. This change was done to avoid the influence that batch normalization has on robustness (Galloway et al., 2019). For binary datasets, reported results used a single output for the classifier. Further details on hyperparameters specific to each dataset are given in Table S1.

For the CIFAR-10 dataset, a few aspects were modified to improve accuracy:

- the first convolutional layer of Resnet-18 was changed to have a  $3 \times 3$  kernel, a stride of 1, and no max pooling immediately after it;
- Resnet-18 convolutional weights were initialized using the Kaiming uniform initialization (He et al., 2015) instead of ImageNet pre-trained weights;
- we used a stochastic gradient descent optimizer, with learning rate equals to 0.01;
- we only checked for best epoch after 33 epochs of training, because of instabilities in the calculated validation robustness before validation accuracy is stable;
- batch normalization was left turned on.

The generator for the direct method for estimating  $\Delta x$  used a U-net (Ronneberger et al., 2015) architecture. In the U-net, we utilized two levels of downsampling for MNIST-3/5

and four levels of downsampling for *Squares* and *COPD*. For training the U-net, we used  $\lambda_G = 0.3$ ,  $\lambda_{RegG} = 0.5$ ,  $\lambda_{Dx} = 1$  and  $\lambda_{D\hat{x}} = 0.01$ . The values of  $-y$  and  $y$  were concatenated as channels to the U-net’s bottleneck. The best epoch during the U-net training was chosen by checking minimal total loss.

The computer infrastructure employed included 11 Titan V, 6 Titan RTX, and 8 Titan V100 SMX2, and all GPUs were used interchangeably depending on availability. Some of the experiments required large GPU memory capacity, which was available only on Titan RTX. Training, combined with best epoch validation, took between 5 minutes and 62 hours for each run, depending on the dataset, method, and GPU used. The average time for each method and dataset are reported in Table S1. Test evaluations for PGD attack took less than 1 hour each. Table S1 also presents further quantitative detail about the datasets used.

The *COPD* dataset was filtered to include only samples for which the PFT was acquired within 30 days of the CXR. Patients with an  $FEV_1/FVC$  lower than 0.7 (Johnson & Theurer, 2014) were assigned to class 1 as having COPD. Images were center-cropped, resized to  $256 \times 256$ , cropped to  $224 \times 224$  (randomly in training), and had their histograms equalized and range adjusted to  $[-1, 1]$ . The dataset was split into training, validation, and test sets by patient ID, since some patients were associated with more than one sample.

### A.2. Proofs

**Theorem 1.** *Let  $\text{sim}(u, v)$  be the alignment between vectors  $u$  and  $v$ , defined by their cosine similarity  $\text{sim}(u, v) = \frac{\langle u, v \rangle}{\|u\|_2 \|v\|_2}$ , let  $m$  be a classification model and let  $c^*(x) := \text{argmin}_{c \neq m(x)} \{\inf \{\|v\|_2 : m(x + v) = c\}\}$ . For a pair of input examples  $x_i$  and  $x_j$ , of different classes  $i$  and  $j$ , respectively, around which  $m$  is locally linear and for which<sup>1</sup>  $\{c^*(x_i), m(x_i)\} = \{i, j\}$  and  $\{c^*(x_j), m(x_j)\} = \{i, j\}$ , the combined robustness  $\rho(x_i) + \rho(x_j)$  of  $m$  is directly proportional to  $\alpha$  according to  $\rho(x_i) + \rho(x_j) = \|x_j - x_i\|_2 \times \alpha$ , where  $\alpha = \text{sim}(x_j - x_i, \nabla \text{logit}(x_i)_j - \nabla \text{logit}(x_i)_i) = \text{sim}(x_i - x_j, \nabla \text{logit}(x_j)_i - \nabla \text{logit}(x_j)_j)$ .*

*Proof.* Since we assume local linearity, the model can be represented by  $\text{logit}(x) = W^T x + b$  by using Lemma 1. Since  $\{c^*(x_i), m(x_i)\} = \{i, j\}$  and  $\{c^*(x_j), m(x_j)\} = \{i, j\}$ , the only two classes involved in the calculation of robustness for both  $x_i$  and  $x_j$  are  $i$  and  $j$ , i.e. the robustness is always measured between input example and decision boundary separating  $i$  and  $j$ . We can then represent  $\text{logit}(x) = W^T x + b$  as a binary model to cal-

<sup>1</sup>The notation of these two equations uses sets, where  $\{a, b\} = \{i, j\}$  means that either  $a = i$  and  $b = j$ , or  $a = j$  and  $b = i$ .

Table S1. Details about datasets and training setup. ART stands for average running time (in hours), and %<sub>-1</sub> for percentage of samples from class -1. The reported ART might be longer than usual runs, since sometimes more than one script was run in the same GPU at the same time.

Properties\Dataset	Spheres	Squares	MNIST-3/5	COPD	MNIST	CIFAR-10	Squares32
TRAIN SET SIZE	10,000,000/EPOCH	10,000	10,397	3,711	54,000	45,000	10,000
VALIDATION SET SIZE	200	200	1,155	596	6,000	5,000	200
TEST SET SIZE	1,000	1,000	1,902	950	10,000	10,000	1,000
DATA DIMENSIONALITY	500	224×224	28×28	224×224	28×28	32×32×3	32×32
% <sub>-1</sub> TRAINING SET	~50%	49.7%	53.1%	63%	-	-	49.7%
% <sub>-1</sub> VALIDATION SET	~50%	50.5%	53.1%	49.8%	-	-	50.5%
% <sub>-1</sub> TEST SET	~50%	48.6%	53.1%	58.2%	-	-	48.6%
PGD - $\epsilon$ FOR TRAINING	0.005	0.2	0.3	0.006	0.3	0.01	-
PGD - $\eta$	0.002	0.02	0.02	0.02	0.02	0.02	-
# EPOCHS	80	30	30	30	30	100	-
$\lambda_\alpha$	0.1	0.1	0.1	10	0.3	0.3	-
$\lambda_{Regz}$	-	-	-	-	1.5	0.03	0.03
BATCH SIZE	50	12	12	12	64	128	-
ART BASELINE	2.3	1.3	4.1	3.7	6.5	15.5	-
ART GAN	3	0.8	0.1	1	61.7	54.7	3.2
ART $L_\alpha$	6.2	1.5	3.7	4.2	6.0	13.1	-
ART PGD	15.4	2.5	3.1	4.9	9.1	27.0	-
ART SQUARE ATTACK	0.3	6.3	8.8	3.8	15.7	17.1	-

culate robustness, given by  $\text{logit}_b(x) = \langle w, x \rangle + b_b = \text{logit}(x)_j - \text{logit}(x)_i$ , and where positive outputs are equivalent to outputting class  $j$ . We note that  $w = W_{:,j} - W_{:,i} = \nabla \text{logit}(x)_j - \nabla \text{logit}(x)_i = \nabla \text{logit}(x)_j - \nabla \text{logit}(x)_i$  and that  $b_b = b_j - b_i$ . The alignment can be simplified as

$$\begin{aligned} \alpha &= \text{sim}(x_j - x_i, \nabla \text{logit}(x)_j - \nabla \text{logit}(x)_i) = \\ &= \text{sim}(x_j - x_i, w) = \frac{\langle x_1, w \rangle - \langle x_0, w \rangle}{\|x_j - x_i\|_2 \|w\|_2}. \end{aligned} \quad (20)$$

If  $x$  is correctly classified,  $\rho(x)$  is equal to the distance between  $x$  and the decision boundary. In the case of misclassification, we use the negative of the distance. We can use the equation of signed distance between  $x$  and the hyperplane defined by  $\langle w, x \rangle + b_b = 0$  and the result from (20) to get

$$\rho(x_i) = -\frac{\langle x_i, w \rangle + b_b}{\|w\|_2}, \quad \rho(x_j) = \frac{\langle x_j, w \rangle + b_b}{\|w\|_2}, \quad (21)$$

$$\rho(x_i) + \rho(x_j) = \frac{\langle x_j, w \rangle - \langle x_i, w \rangle}{\|w\|_2} = \alpha \times \|x_j - x_i\|_2. \quad (22)$$

□

**Theorem 2.** Assuming that, for a multi-class dataset of classes  $C$ ,

1. it is possible to define  $K$  mutually exclusive sets  $\mathcal{S}_k$ , each containing regions of the supports of two classes

$i_k$  and  $j_k$ , where  $\bigcup_{c \in C} \text{supp}_c = \bigcup_{k=1}^K \mathcal{S}_k$ , i.e., they cover the whole space of the support of classes;

2. for each  $\mathcal{S}_k$ , it is possible to define a bijection between the respective regions of support of classes  $i_k$  and  $j_k$  such that, given all bijection pairs  $(x_{i_k}, x_{j_k})$ ,  $x_{i_k} \in \text{supp}_{i_k}$  and  $x_{j_k} \in \text{supp}_{j_k}$ ,

$$(a) \quad P(x_{i_k}) = P(x_{j_k}),$$

(b) a decision model  $m$  is locally linear around  $x_{i_k}$  and  $x_{j_k}$ ;

$$(c) \quad \{c^*(x_{i_k}), m(x_{i_k})\} = \{i_k, j_k\} \quad \text{and} \quad \{c^*(x_{j_k}), m(x_{j_k})\} = \{i_k, j_k\};$$

then the expected robustness of  $m$ ,  $\rho_m$ , is related to the expected alignment  $\bar{\alpha}$  between  $\nabla_{\ell(x)}$  and  $\Delta x$  of pairs  $(x_{i_k}, x_{j_k})$  over all  $\mathcal{S}_k$ , according to

$$\rho_m \geq \frac{\inf(\mathcal{D}) \times \bar{\alpha}}{2} \quad \text{and} \quad \bar{\alpha} \geq \frac{2 \times \rho_m}{\sup(\mathcal{D})}, \quad (7)$$

where  $\mathcal{D}$  is the set of distances  $\|x_{i_k} - x_{j_k}\|_2$  over all pairs  $(x_{i_k}, x_{j_k})$  over all  $\mathcal{S}_k$ .

*Proof.* The expected robustness of a model  $m$  can be written as

$$\rho_m = \sum_{c=1}^C \int_{\text{supp}_c} P(x) \rho(x) dx = \sum_{k=1}^K \int_{\mathcal{S}_k} P(x) \rho(x) dx. \quad (23)$$



Since we can establish a bijection in each  $\mathcal{S}_k$  between  $\text{supp}_{i_k}$  and  $\text{supp}_{j_k}$ , we can integrate over both supports at the same time, pair by pair of  $x_{i_k}$  and  $x_{j_k}$ . Since  $P(x_{i_k}) = P(x_{j_k})$ , we can factor the probability, resulting in

$$\rho_m = \sum_{k=1}^K \int_{\text{supp}_{i_k}, \text{supp}_{j_k}} P(x_{i_k})(\rho(x_{i_k}) + \rho(x_{j_k})) dx. \quad (24)$$

It is worth noting that sampling is balanced between the two classes in  $\mathcal{S}_k$  since, from the established bijection,

$$\int_{\text{supp}_{i_k}} P(x) dx = \int_{\text{supp}_{j_k}} P(x) dx = \frac{1}{2} \int_{\mathcal{S}_k} P(x) dx. \quad (25)$$

Using Theorem 1 to substitute for  $\rho(x_{i_k}) + \rho(x_{j_k})$  and using (25),

$$\begin{aligned} \rho_m &= \sum_{k=1}^K \int_{\text{supp}_{i_k}, \text{supp}_{j_k}} P(x_{i_k}) \alpha_{i_k} \|x_{i_k} - x_{j_k}\|_2 dx \geq \\ &\geq \sum_{k=1}^K \inf(\mathcal{D}) \int_{\text{supp}_{i_k}} P(x_{i_k}) \alpha_{i_k} dx = \\ &= \frac{\inf(\mathcal{D})}{2} \int_{\mathcal{S}_k} P(x) \alpha dx = \frac{\inf(\mathcal{D}) \times \bar{\alpha}}{2}, \end{aligned} \quad (26)$$

$$\begin{aligned} \rho_m &= \sum_{k=1}^K \int_{\text{supp}_{i_k}, \text{supp}_{j_k}} P(x_{i_k}) \alpha_{i_k} \|x_{i_k} - x_{j_k}\|_2 dx \leq \\ &\leq \sum_{k=1}^K \sup(\mathcal{D}) \int_{\text{supp}_{i_k}} P(x_{i_k}) \alpha_{i_k} dx = \\ &= \frac{\sup(\mathcal{D})}{2} \int_{\mathcal{S}_k} P(x) \alpha dx = \frac{\sup(\mathcal{D}) \times \bar{\alpha}}{2}, \quad \bar{\alpha} \geq \frac{2 \times \rho_m}{\sup(\mathcal{D})}. \end{aligned} \quad (27)$$

□

### A.3. Details of the indirect generation of $\widehat{\Delta x}$

The code for the cGAN used in the experiments was cloned from <https://github.com/ilyakava/BigGAN-PyTorch>. We only added support for loading the MNIST and *Square32* dataset and removed the fixed random seed.

Considering the optimization to find  $z_c^*$ , the hyperparameters were selected from a visual check of the proximity of the images to their original class and the representation of the destination class. During its optimization,  $z$  was initialized to the zero vector. The first 600 iterations were calculated with  $\lambda_{Regz} = 0$  to facilitate the optimization process. The

Table S2. Baseline alignment metric ( $\bar{\alpha}_x$ ) values when considering distinct functions in the gradient ( $\Psi := \text{logit}(x)$ ). In bold, the metric we reported, coinciding with the highest values.

SETUP	$\Psi_{\bar{c}} - \Psi_y$	$\Psi_{c^*} - \Psi_{m(x)}$	$\Psi_y$	$\Psi_{m(x)}$
M-B	0.036	0.036	0.038	<b>0.038</b>
M- $L_\alpha$	0.267	0.267	0.320	<b>0.320</b>
M-P	0.030	0.030	0.043	<b>0.043</b>
C-B	0.008	0.008	0.008	<b>0.008</b>
C- $L_\alpha$	0.018	0.018	0.019	<b>0.020</b>
C-P	0.029	0.029	0.031	<b>0.031</b>

following 150 iterations were calculated with  $\lambda_{Regz} \neq 0$ . This two-step optimization process allowed for using a single optimization per pair  $(x_k, c)$ , instead of several random initializations for  $z$  to avoid local minima. Optimization over  $z$  was performed using the Adam optimizer (Kingma & Ba, 2015), with learning rate 0.1 for CIFAR-10 and 0.2 for MNIST and *Square32*.

### A.4. Additional images generated for gradient estimation

Figure S1, Figure S2, Figure S3, Figure S4, Figure S5, and Figure S6 show a set of examples for the results of the methods proposed in Section 2.3.

### A.5. Comparison of baseline alignment metric with several input gradients

Table S2 shows that the provided baseline metric corresponds to the highest alignment value when comparing several methods of calculating the input gradient.

### A.6. Correlation between alignment and robustness for a fixed training method

Figure A.6 shows alignments for a fixed training method (PGD) and varying robustness, controlled by  $\epsilon$ .

### A.7. Robustness graphs

In Figure S8, all attacks with a large enough bound were able to get 100% success, and increasing the perturbation norm  $\epsilon$  increased attack success rate, signs that gradient does not suffer from intensive gradient obfuscation (Athalye et al., 2018) in any of the methods. For the *Squares* dataset, the alignment penalty training method showed some gradient obfuscation for one of the classes, as seen in the bottom gap between black-box attack and PGD attack in Figure S8, without largely reflecting on the numbers of Table 2.

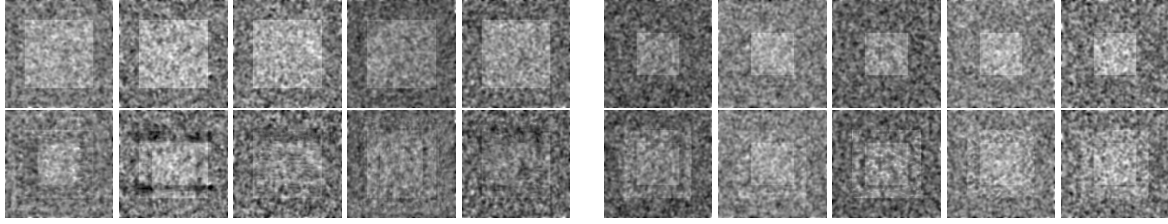


Figure S1. Examples of generated  $\hat{x}'$  for the *Squares* dataset through the direct method. The top row contains the original image  $x$ , and the bottom row contains the generated  $\hat{x}'$ . There are five columns per class of  $x$ .

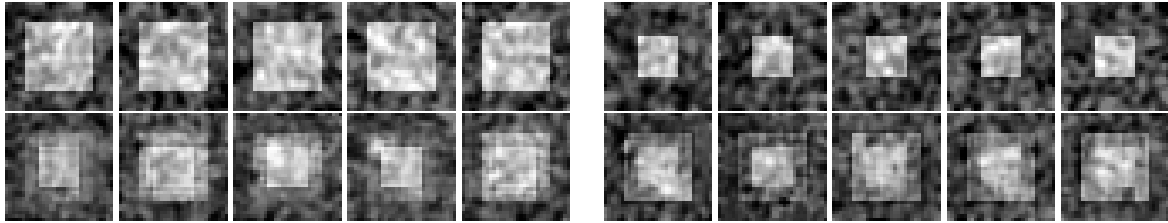


Figure S2. Examples of generated  $\hat{x}'$  for the *Squares32* dataset through the indirect method. The top row contains the original image  $x$ , and the bottom row contains the generated  $\hat{x}'$ . There are five columns per class of  $x$ .

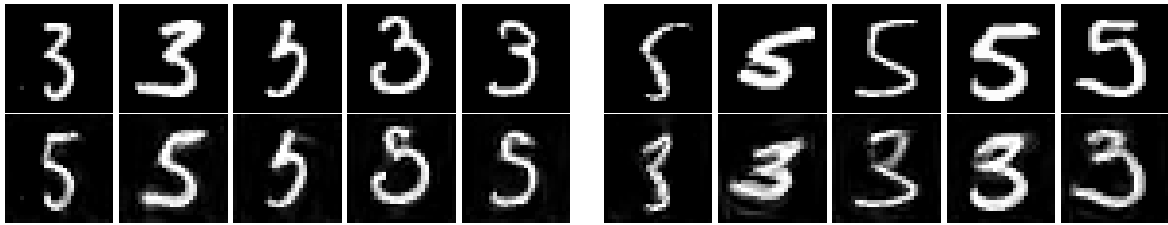


Figure S3. Examples of generated  $\hat{x}'$  for the MNIST-3/5 dataset through the direct method. The top row contains the original image  $x$ , and the bottom row contains the generated  $\hat{x}'$ . There are five columns per class of  $x$ .

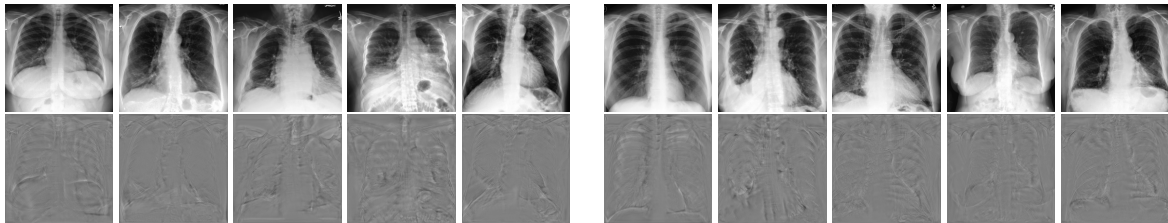


Figure S4. Examples of generated  $\hat{x}'$  for the *COPD* dataset through the direct method. The top row contains the original image  $x$ , and the bottom row contains the generated  $\hat{\Delta}x$ . There are five grouped columns per class of  $x$ , from left to right: class -1, class 1. We show  $\hat{\Delta}x$  because changes are small and difficult to perceive in  $\hat{x}'$ .

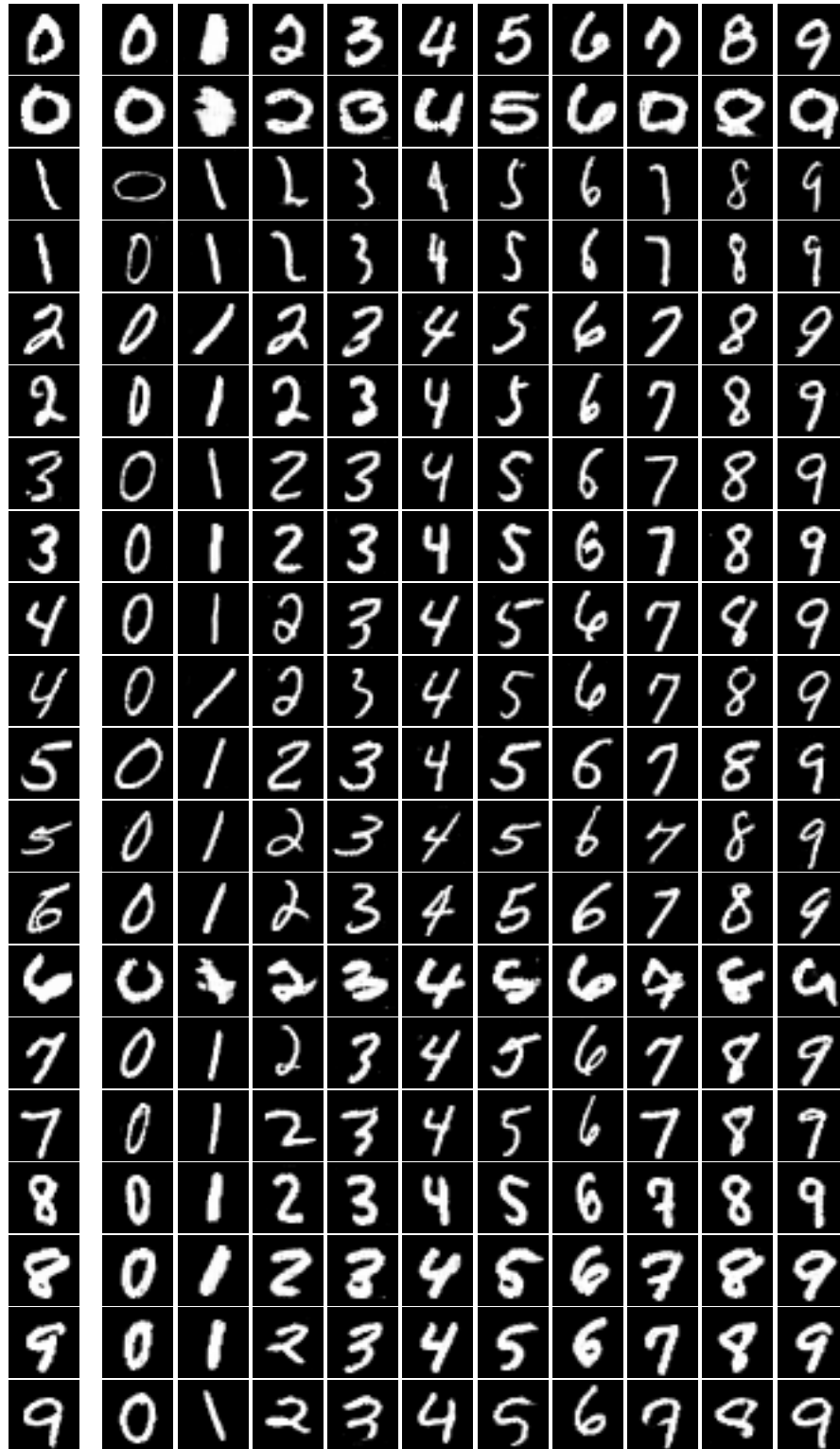


Figure S5. Examples of generated  $\hat{x}'$  for the MNIST dataset through the indirect method. There are two rows per class of  $x$  (left column), and 10 columns on the right of  $x$  to represent each of the 10 destination classes.

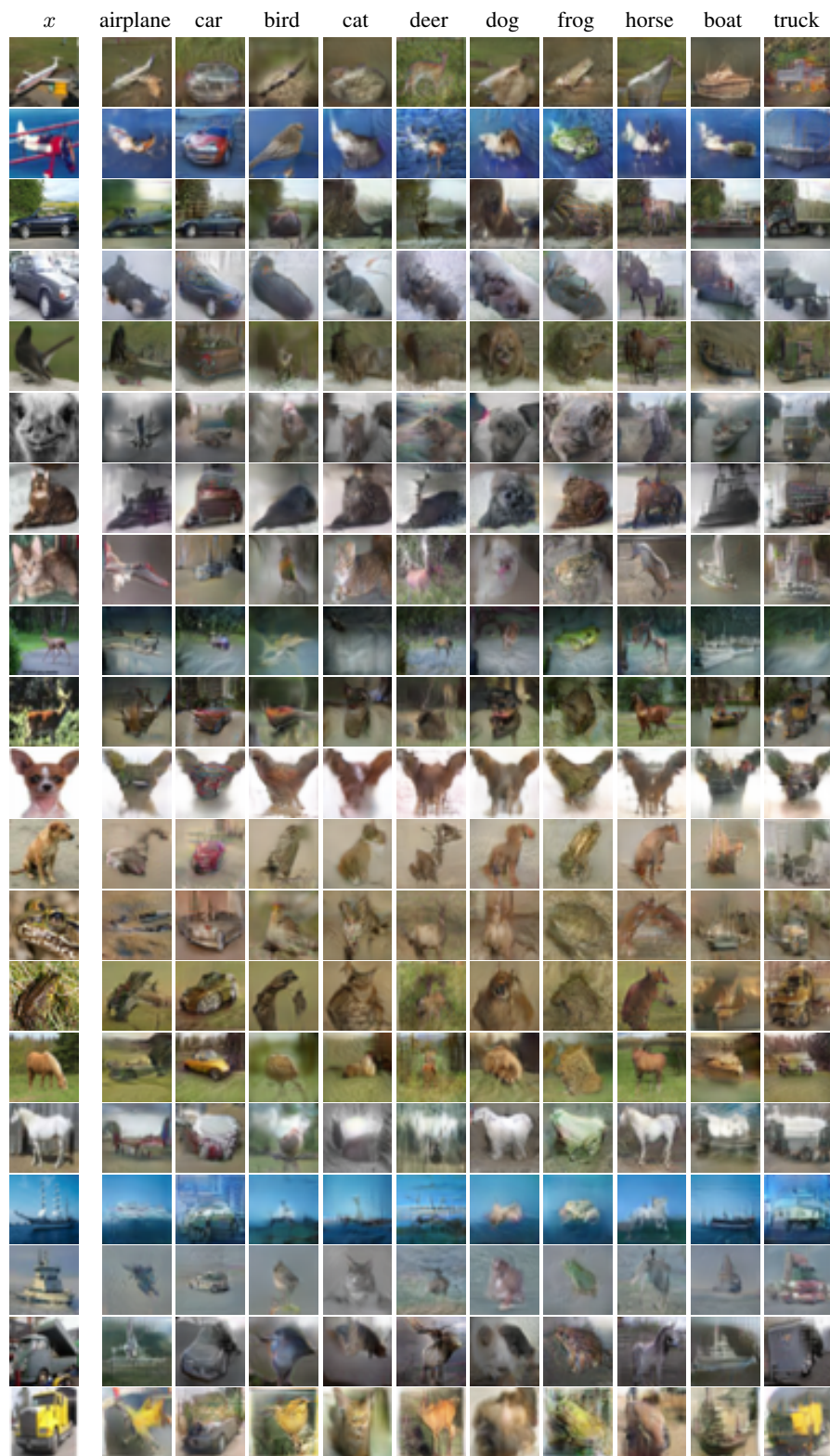


Figure S6. Examples of generated  $\hat{x}'$  for the CIFAR-10 dataset through the indirect method. There are two rows per class of  $x$  (left column), and 10 columns on the right of  $x$  to represent each of the 10 destination classes. Classes are, from top to bottom and left to right: airplane, car, bird, cat, deer, dog, frog, horse, boat, truck.



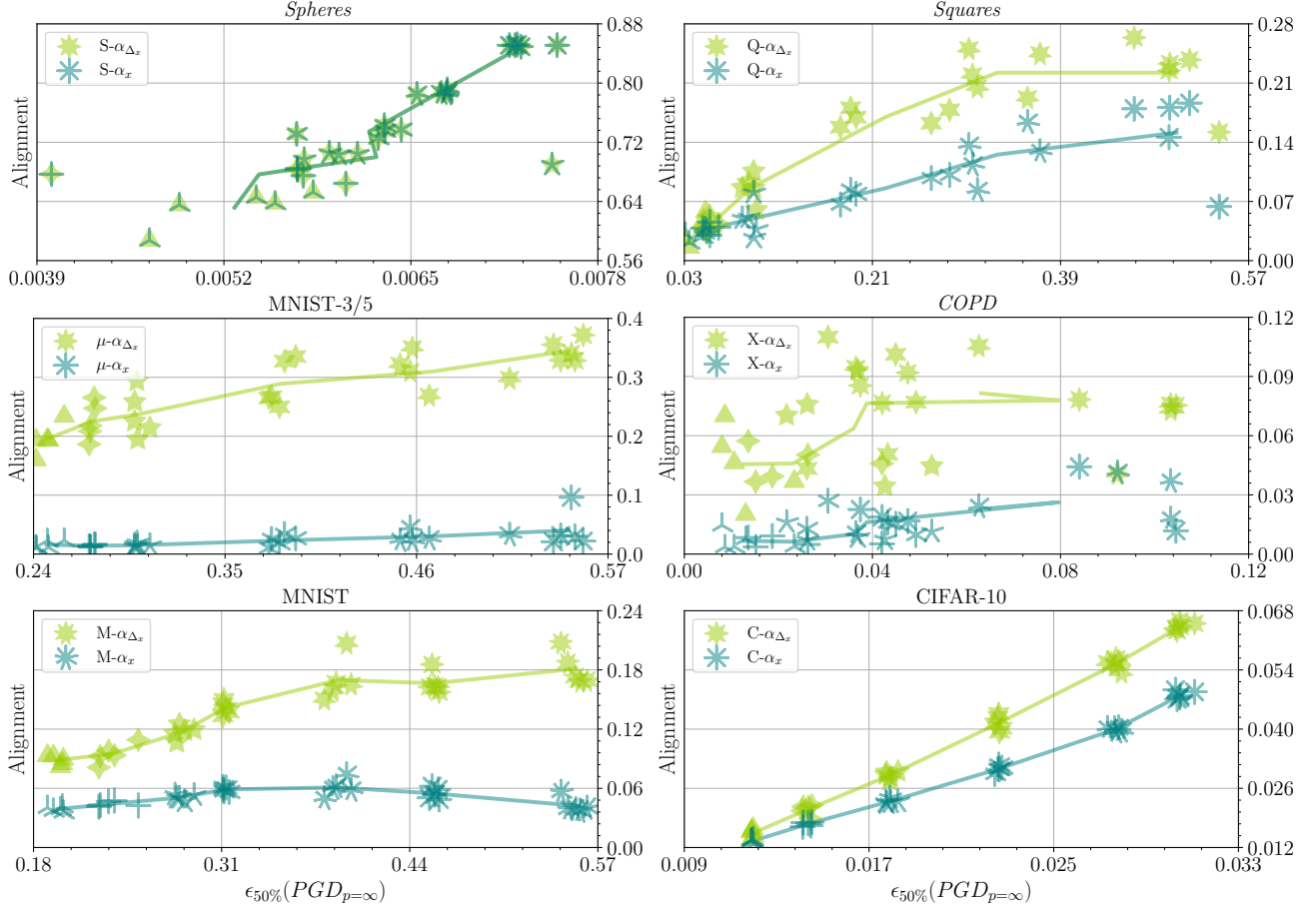


Figure S7. Alignment vs.  $L_\infty$  robustness for PGD-trained models. Star-like symbols represent our proposed alignment, and asterisk-like symbols represent baseline alignments. For each dataset, the higher the number of spikes/points in a symbol, the higher the value of  $\epsilon$  used for PGD-training. There are five models for each  $\epsilon$ . The line connects the average coordinates of each group of 5 models with fixed  $\epsilon$ , ordered by  $\epsilon$ .

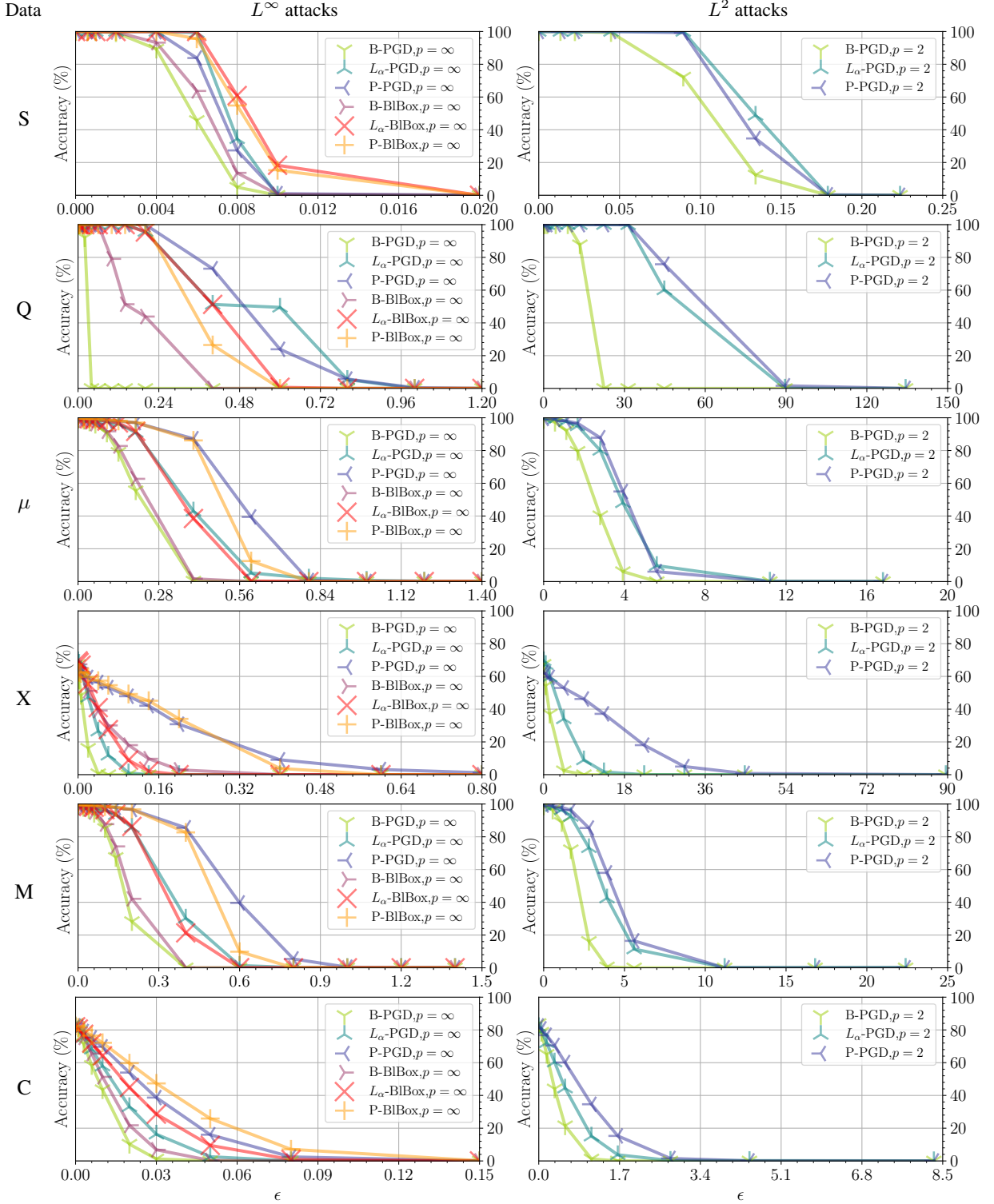


Figure S8. Accuracy of models as a function of perturbation norm  $\epsilon$  after training using a plain supervised training baseline (B), alignment penalty ( $L_\alpha$ ), and adversarial training with PGD (P) for 6 datasets: *Spheres* (S), *Squares* (Q), MNIST-3/5 ( $\mu$ ), *COPD* (X), MNIST (M), CIFAR-10 (C). We report results for 3 attacks: PGD (Madry et al., 2018) restricted by the  $L^\infty$  norm, the black-box Square Attack (Andriushchenko et al., 2020) (BiBox) restricted by the  $L^\infty$  norm, and PGD (Madry et al., 2018) restricted by the  $L^2$  norm. Models were selected randomly from the 5 trained models for each training setup.